A K-BAND SENSOR INTERFACE DESIGN FOR REMOTE CARDIORESPIRATORY SENSING AND MONITORING

by

Ali Kiaghadi

B.S., Electrical Engineering, University of Tehran, 2012

Submitted to the Institute for Graduate Studies in
Science and Engineering in partial fulfillment of
the requirements for the degree of
Master of Science

Graduate Program in Electrical and Electronics Engineering
Boğaziçi University
2015

A K-BAND SENSOR INTERFACE DESIGN FOR REMOTE CARDIORESPIRATORY SENSING AND MONITORING

APPROVED BY:

Assis. Prof. Ahmet Öncü (Thesis Supervisor)	....
Assoc. Prof. Şenol Mutlu	....
Prof. Cengizhan Öztürk	....

DATE OF APPROVAL: 06.08.2015

ACKNOWLEDGEMENTS

It has been two years since I started working on this project and there were lots of people who helped me complete my thesis. Here I would like to express my gratitude to the institutions and people that contributed to this work, directly or indirectly, and thus took part in its making.

The works in this thesis have been supported by TÜBİTAK (112E170).

I would like to thank my supervisor Ahmet Öncü for his invaluable experience and guidance, and also to my respectable jury members Cengizhan Öztürk and Şenol Mutlu for their stimulating evaluation of the work.

I would also like to thank my friend and lab member, Günay Turan, who helped me a lot during this period and made a friendly environment in RF IC Lab where we developed the project and did the measurements.

The person who helped me the most in the beginning of my journey in Turkey was Ramin Fadaei Fouladi, who also helped me get settled and familiar with the new environment. I also want to thank Berk Camli who helped my in writing the thesis. In addition, I want to thank Berkay Enginoğlu and Doğansel Teker, who worked on their Bachelor's thesis in RF Lab and whose efforts made contribution to my project. I also thank Mohammad Beygi, Pooya Yousefi, Amin Delparish, Sina Talebi, Farhad Kazemi Khosroshahi, and Kaan Oktay for their contribution to our measurements.

Last but most definitely not the least, my deepest gratitude is to my family members who showed me the path to knowledge my whole life, and to my supportive wife, Nazanin Takbiri, whose words always encouraged me to reach my goals since the day I met her and supported me during this project. That is the reason I am dedicating this work to her.

ABSTRACT

A K-BAND SENSOR INTERFACE DESIGN FOR REMOTE CARDIORESPIRATORY SENSING AND MONITORING

The need for a contact-less cardiorespiratory measurement made many researchers put their efforts on this matter. There are many different approaches to this issue. From flow of the air in and out of the mouth [1] to image processing of a camera [2]. A technique based on Doppler effect to detect movement in patient's chest wall is used. This movement contains many different kinds of data such as breathing movement, heartbeat, and random muscle twitches. In addition, we receive signal from stationary environment as well as dynamic objects and people around the patient. That is the reason why we need to precisely filter out the unwanted data in order to obtain the bio-signals successfully. A system has been designed and its functionality tested. An analog circuit manages the input signal coming from the K-band sensor. Filtering and amplification are done in this block. An automatic gain control (AGC) unit is also designed and used to maintain the output signal amplitude so that we can use the highest efficiency possible from analog to digital converter (ADC). The signal is then converted to digital and the relative movement is calculated in an arm-based processor. Then, the data are sent to the monitoring terminal using user datagram protocol (UDP). In the monitoring terminal, several digital signal processing steps are taken to visualize the signal in time domain, frequency domain, and spectrogram. A graphical user interface (GUI) is designed for easier observation of life signs. Additionally, three similar systems are fabricated and placed in three different locations, all of them connected to a server. This makes it possible to monitor the conditions of multiple patients at the same time and using this idea, we created a medical hub, which can be placed in a hospital to help monitor patients inside their home or in different rooms in hospital.

ÖZET

KALP VE SOLUNUM VERİLERİN UZAKTAN ALGILANMASI VE GÖRÜNTÜLENMESİ AMAÇLI K-BAND SENSÖR SİSTEMİ ARAYÜZ TASARIMI

Kalp ve solunum ile ilgili verilerin temassız ölçülmesine duyulan ihtiyaç birçok araştırmacıyı bu konuda çalışmaya sevk etmektedir. Temassız ölçüm çalışmaları için ağızdan çıkan hava akımının ölçülmesinden kamera görüntülerinin işlenmesine kadar birçok farklı yaklaşım kullanılmıştır. Bu tez çalışmasında ise Doppler etkisi ile hastanın göğüs kafesindeki hareketin saptanması tekniği baz alınmıştır. Hastanın göğüs kafesindeki bu hareket nefes alıp verme hareketi, kalp atışı verilerini içerisinde barındırmaktadır. Bu verilere ek olarak çevredeki hareketli objelerden ve durağan çevreden kaynaklı veriler de kalp ve solunum verileri ile beraber sisteme girmektedir. Bu nedenle, biyolojik verilerin başarılı bir şekilde elde edilebilmesi için istenmeyen verilerin filtrelenmesi gerekmektedir. Bütün bu gereksinimleri karşılamak amacıyla bir sensör sistemi tasarlanmış ve işlevselliği test edilmiştir. K-Band sensörden gelen giriş sinyali analog bir devre aracılığıyla işlenmektedir. Sinyalin filtrelenme ve kuvvetlendirilme işlemleri de bu bloğun içinde yapılmaktadır. Analog veriden sayısal veriye çevirici devrenin mümkün olan en yüksek verimde çalışabilmesi için gereken çıkış işareti genliğinin sağlanabilmesi için de bir otomatik kazanç kontrol birimi tasarlanmıştır. Dijital veriye çevrilen bu çıkış işareti, ARM tabanlı bir işlemci yardımıyla dijital olarak işlenerek göreli hareket hesaplanmıştır. Bu işlemin ardından çıkan veri, UDP kullanılarak görüntüleme terminaline gönderilmiştir. Görüntüleme terminalinde veriyi zaman uzayında, frekans uzayında ve spektogramda görselleştirebilmek için birtakım işaret işleme teknikleri kullanılmıştır. Bütün bu sistemden 3 adet üretilmiştir. Üretilen 3 sistem farklı noktaya yerleştirilmiş ve aynı sunucu üzerinde 3 farklı hastanın eş zamanlı takibi mümkün kılınmıştır. Bu özellikten yola çıkılarak, hastanelerde ya da evlerde farklı lokasyonlardaki hastaların yaşam sinyalleri eş zamanlı olarak gözlemlenebilir.

TABLE OF CONTENTS

LIST OF FIGURES

LIST OF TABLES

LIST OF SYMBOLS

C	Capacitor/capacitance
D	Diode
f_0	Natural frequency
f_{3dB}	3dB cut-off frequency
$I(t)$	In-phase signal
$Q(t)$	Quadrature signal
R	Resistor/resistance
$r(t)$	Relative movement of the object in front of the sensor
R_x	Receiving antenna
T_x	Transmitting antenna
V_{fm}	Forward voltage of diode
λ	Radar wavelength
$\phi(n)$	Phase shift induced by noise
$\phi(t)$	Phase shift induced by range motion.
ϕ_0	Phase shift induced by static objects

LIST OF ACRONYMS/ABBREVIATIONS

AC	Alternating Current
ADC	Analog to Digital Converter
AGC	Automatic Gain Control
AIDS	Acquired Immune Deficiency Syndrome
ARM	Advanced RISC machines
BPF	Band-Pass Filter
BPM	Beats Per Minute
BW	Band Width
CAD	Computer-Aided Design
CHF	Congestive Heart Failure
CMOS	Complementary Metal-Oxide-Semiconductor
COPD	Chronic Obstructive Pulmonary Disease
CT	Computed Tomography
DC	Direct Current
ECG	ElectroCardiogram
EM	ElectroMagnetic
FCC	Federal Communications Commission
FFT	Fast Fourier Transform
GPIO	General-Purpose Input/Output
GSM	Global System for Mobile communications
HIV	Human Immunodeficiency Virus
HPF	High-Pass Filter
IC	Integrated Circuit
IF	Intermediate Frequency
IP	Internet Protocol
LAN	Local Area Network
LIDAR	LIght Detection and Ranging
LNA	Low-Noise Amplifier

LPF	Local-Pass Filter
MRI	Magnetic Resonance Imaging
NFFT	Number of Fast Fourier Transform
OPAMP	OPerational AMPlifier
OTA	Operational Transconductance Amplifier
PCB	Printed Circuit Board
RADAR	RAdio Detection And Ranging
RF	Radio Frequency
RR	Respiratory Rate
SMD	Surface-Mount Device
SNR	Signal-to-Noise Ratio
UDP	User Datagram Protocol
VGA	Variable Gain Amplifier
WHO	World Health Organization
WLAN	Wireless Local Area Network

1. INTRODUCTION

1.1. Radar Frequency Bands

According to the world health organization (WHO), cardiovascular diseases are the largest causes of death all around the world [3, 4]. Monitoring respiration and heart rate can significantly help diagnosis of such diseases. To do this, there exist a wide range of instruments available to the medical personnel.

The most commonly used tool in heartbeat monitoring is the electrocardiogram (ECG), which monitors the electrical activity of the heart. Large and expensive magnetic resonance imaging (MRI) and computed tomography (CT) machines can also do the same and can provide detailed images of the entire human body. Various methods also exist to detect respiration rate. Respiration measurement belt is a conventional way of doing so, which may be uncomfortable for many cases of patients and may also affect the natural respiration rate. Recently, there have been several works presenting non-invasive detection methods for respiration; from using image processing tools on real time video of the patient's body [2] to detecting flow of the air in and out of the patient's mouth [1] are some of the proposed methods. Another proposed method for vital signs detection is using radar devices.

Radar, which was originally an acronym for radio detection and ranging, has a rich history behind it which starts with Heinrich Hertz's experiments in the 1880's [5]. Today, radar systems exist for a variety of applications from weather observation to guidance systems and law enforcement.

Radar systems operate over a wide range of frequencies, often considered to be between 300 MHz and 300 GHz [6]. In the past, systems were usually designed to work in 100 MHz to 36 GHz range; however, systems also exist that work below or above these range, from few megahertz up to hundreds of gigahertz frequency which are also known as millimeter-wave signals, meaning their wavelengths are on the order of a millimeter [5]. Impulse, or carrier-free, radars operate down to frequencies on the order of 1 MHz [7] and light detection and ranging (LIDAR) systems operate in the optical range [8].

The microwave spectrum is subdivided into bands, as noted in Table 1.1. Transmission in the electromagnetic (EM) spectrum is regulated by government bodies, such as the federal communications commission (FCC) in the United States. A radio license is required to operate a microwave system in most of the EM spectrum. However, there are some bands free for experimental usages.

Table 1.1. IEEE standard radio frequency (RF) letter-band nomenclature.

Band designation	Nominal frequency range
HF	$3 - 30MHz$
VHF	$30 - 300MHz$
UHF	$300 - 1000MHz$
L	$1 - 2GHz$
S	$2 - 4GHz$
C	$4 - 8GHz$
X	$8 - 12GHz$
$\mathrm{K_u}$	$12 - 18GHz$
K	$18 - 27GHz$
$\mathrm{K_a}$	$27 - 40GHz$
V	$40 - 75GHz$
W	$75 - 110GHz$
mm	$110 - 300GHz$

We tried to choose a frequency band which is free to use and is not occupied by other applications such as GSM or WLAN. Higher frequencies are more suitable for lower distances since their penetration range is shorter. However, they offer a higher signal to noise ratio and more sensitivity. Lower frequencies therefore are used in applications such as finding bodies trapped under rubble. 24 GHz frequency has λ

(wavelength) of 12.5 mm which makes it possible to be integrated on a chip later on.

1.2. Using Doppler Radar for Biomedical Purposes

One way of using the concept of radar in vital signs detection is using Doppler effect. According to Doppler effect, the frequency of the wave reflected from a surface changes as the surface moves. As a result, the reflected wave has information regarding movement of the surface in its phase. The mathematical expressions and algorithm used to calculate relative movement is described in following chapters. Microwave Doppler radar has been used for wireless sensor applications for many years. Since this method of sensing is unobtrusive, it has attracted attention for new application on human health-care. Doppler radar is being used in some other applications as well. Finding bodies under rubble caused by earthquake [9], volume change sensing, and sleep apnea syndrome detection can be counted as some other applications where Doppler radar can be used. This method is more efficient when patient has burnt skin or we are dealing with early born infants or and elderly, since contact with their body can be harmful or uncomfortable. This has been worked for some years now and many researchers came up with their ideas on how to use Doppler effect in detecting vital signs. Works done in [10–13] are based on the same concept, which is using Doppler radar in movement detection, which in this case contains information regarding respiration and heart rate. However, each of them has its own drawbacks and issues. Static range, inability to detect behind thin barriers, such as glass, thin wood, etc, and lack of a warning system are some of the issues regarding those works.

An important plus point of this work in comparison with the previous works is the fact that a health-care server is implemented to monitor different patients simultaneously (Figure 1.1). Using the Internet, all radar terminals are connected to the main server, which can be placed in a hospital, where the care taker can easily monitor his/her patients. Also, the gain of the system is no longer constant, as a result of adding an automatic gain control unit (AGC) in the analog circuitry, the output amplitude is obtained regardless of the distance between the radar and the patient. The flexibility in distance between the system and patient is another advantage of this work, which can reach up to 7 meters [14]. In most of the previous works, this number could reach up to 2 meters.

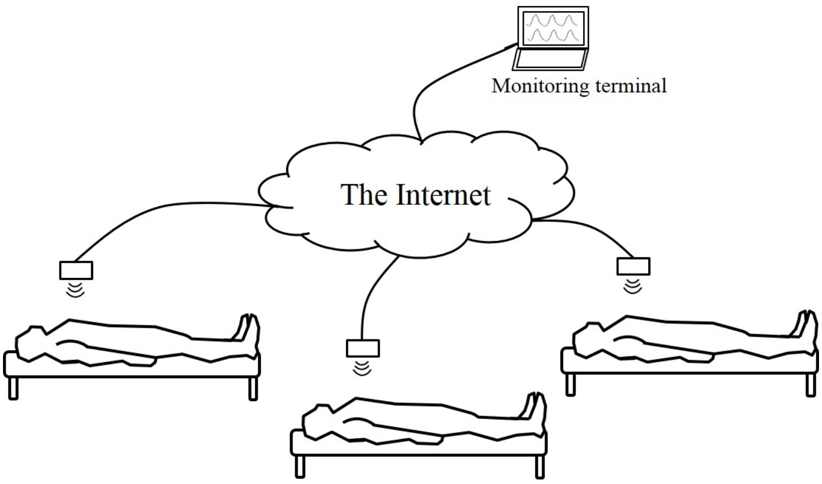

Figure 1.1. Different systems send their data to the main server for processing, altogether creating a health-care network.

The final goal would be to visualize the data so it can be easily understandable. We can have a record of patient's medical data. Useful data can include breathing pattern of the patient, breathing rate, heart rate, and changes of these parameters through time. Digital signal processing steps are required to extract these informations.

Null-points is a common issue in Doppler radars. This happens every quarter wavelength from the radar to the subject. Since the carrier frequency is relatively high, this problem will severely reduce the detection precision. This is the main reason for using in-phase and quadrature signals.

Figure 1.2. Designed system can detect cardiorespiratory data from behind a thin glass wall, which makes it useful to be used for premature babies.

2. OPERATION PRINCIPLE OF A DOPPLER RADAR

Here is the simplified block diagram of the used sensor. As it shows, it generates the in-phase and quadrature signals which have 90° phase shift relative to each other. Sensor has 45° viewing angle and has a output DC offset that can vary between 1 V to 4 V.

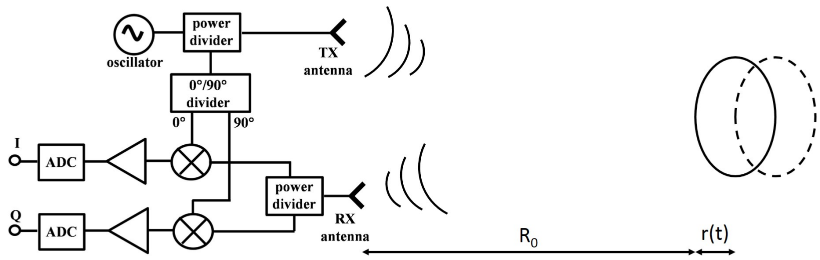

Figure 2.1. Simplified block diagram of the sensor.

Assuming that the normal border of the sensor surface plane is perpendicular to the chest wall, the distance $r(t)$ from the sensor can be calculated as explained here. The relation between phase ($\phi(t)$), wavelength λ, and displacement ($r(t)$) of the subject is shown in Equation 2.1.

$$r(t) = \frac{\phi(t)}{4\pi}\lambda \tag{2.1}$$

However, the signals we obtain from the sensor, the in-phase and quadrature signals, contain the information in a way shown in Equations 2.2 and 2.3.

$$I(t) = cos(\frac{4\pi r(t)}{\lambda} + \phi(n) + \phi_0) \tag{2.2}$$

$$Q(t) = sin(\frac{4\pi r(t)}{\lambda} + \phi(n) + \phi_0) \tag{2.3}$$

Where ϕ(n) represents the noise and ϕ_0 stems from static objects reflecting the incoming sensor waves. Since both of these signals are unwanted, they are counted as noise and we try to eliminate them in pre-amplifier stage. ϕ(n) produces noise in all frequency ranges while ϕ_0 will generate DC offset.

Our aim is to find $r(t)$. In order to find it, we need to divide the quadrature signal to in-phase signal and then take the unwrapped arctangent from the result, as shown in Equation 2.4.

$$r(t) \propto tan^{-1}(\frac{Q(t)}{I(t)}) - \phi(n) - \phi_0 \tag{2.4}$$

An illustration of this method is shown in Figure 2.2. To fulfill the aim of the project,

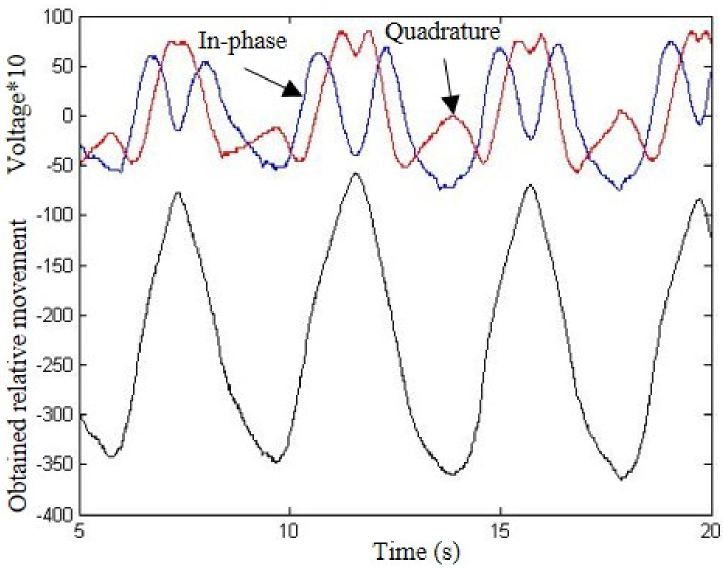

Figure 2.2. In-phase and quadrature signals and the extracted movement data.

the relative movement of the chest can be used and there is no need to exactly calculate the movement. From the extracted relative movement, we have everything we need to calculate the vital signs and monitor the instantaneous changes in them.

3. SYSTEM DESIGN DESCRIPTION

The works done in this project can be categorized in two classes. Hardware implementation and software realization. The hardware part is mainly responsible for getting in-phase and quadrature signals from the sensor and amplify it while maintaining the SNR. Converting from analog to digital is the last step in analog circuitry. However, in digital domain, two main codes are written in Python. They are responsible for the digital signal processing part, which is mathematical derivation of relative movement, phase unwrapping, taking fast Fourier transform (FFT), generating spectrogram, visualizing the signal plots, and so on. one code is running in each ARM-based processor and the other one is running in the monitoring terminal. The general block diagram of the system is shown in Figure 3.1. The transmission medium

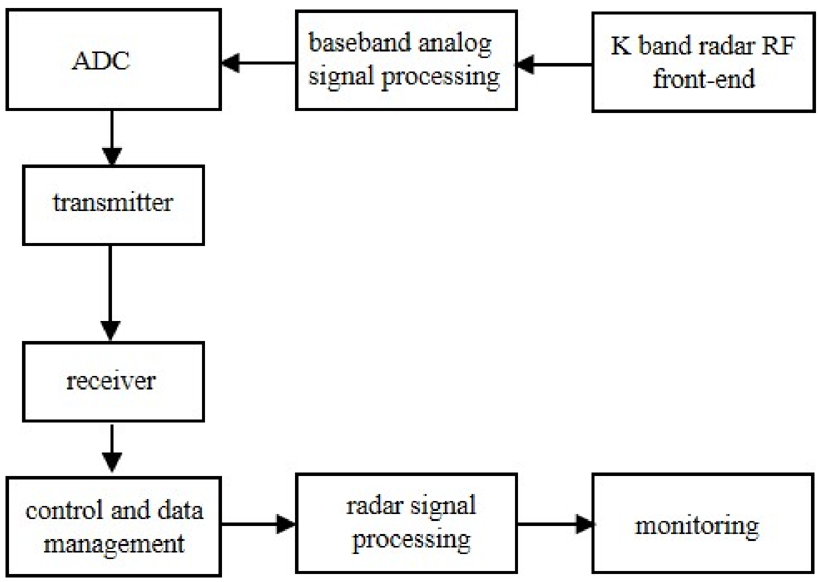

Figure 3.1. Simplified block diagram of the system.

is the Internet. Each block is explained in details and its working principle presented in following sections.

3.1. Analog Circuitry

The output signal of the sensor, contains noise in all frequency ranges. However, the fact that our desired signal is located in lower frequency values, we have to deal with the flicker noise. Flicker noise, also known as $1/f$ noise, can be troublesome in lower frequencies. In the Figure 3.2, which shows the output of the final circuit while monitoring the mechanical respiratory simulator, the flicker noise is clearly visible. As frequency reduces, noise floor's intensity increases. Note that the sparks in the Figure represent the harmonics of the signal stemmed from the surface displacement.

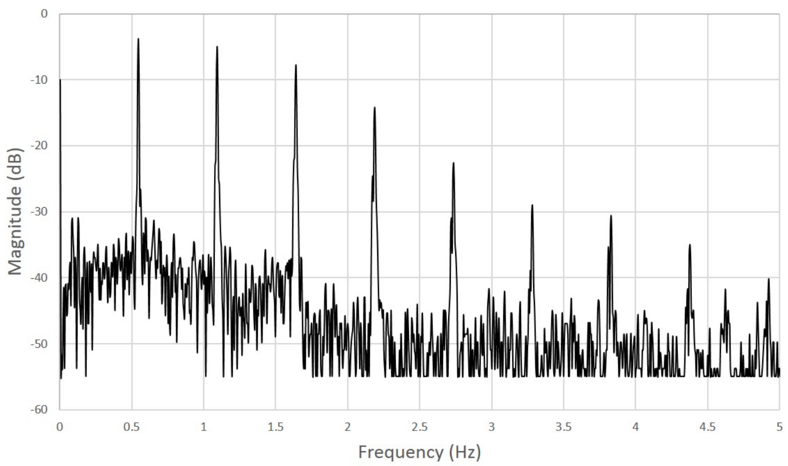

Figure 3.2. As we get closer to DC frequencies, the noise power increases.

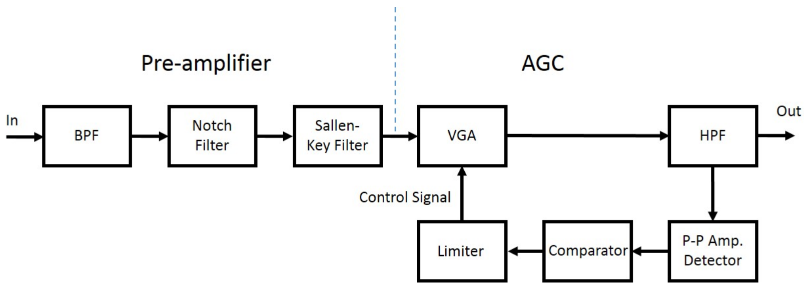

Figure 3.3. Block diagram of the designed analog circuit.

To increase SNR, several low-pass filters (LPF) and high-pass filters (HPF) are placed in signal route to attenuate signals in unwanted frequency ranges. Different filters with different characteristics are used in order to make the signal ready for digitization. In this design, we tried to use fewer blocks with higher efficiency, hence achieving smaller area and lower power consumption. This circuit can be further categorized in to two sub-blocks, pre-amplifier and AGC. The block diagram of the circuit can be seen in Figure 3.3. In the following sections, each block is explained in details. The simulation result for each block and general circuit is presented in Chapter 5.

3.1.1. Pre-amplifier

Blocks placed in this part of the circuit are responsible to increase SNR and amplitude of the signal so that the signal is ready to be converted into digital domain. However, AGC unit is required after pre-amplifier to keep output level at a constant value before the analog to digital converter (ADC).

3.1.1.1. Band Pass Filter. Before amplifying the signal, it is essential to remove the unwanted signals from intermediate frequency (IF) sensor output. Adding a band pass filter (BPF) will increase the SNR. The schematics of the designed BPF is shown in Figure 3.4. The values chosen for the components are stemmed from following equation which determines the higher and lower cut-off frequencies of the filter.

$$f_c = \frac{1}{2\pi RC} \tag{3.1}$$

R_3 and C_2 determine the lower cut-off frequency, while in the active filter, R_2 and C_1 are responsible for higher cut-off frequency. Gain of this stage can be adjusted by changing R_1.

3.1.1.2. Notch Filter. Our environment is surrounded with power cables carrying 50 Hz town electricity. This affects all electrical devices and induces 50 Hz noise in signal traces. Power of this noise is much higher than other noise frequencies and low-pass filters are not enough to attenuate this noise to a desired level. Notch filter is a narrow band-stop filter that rejects the unwanted frequency and does not make any noticeable

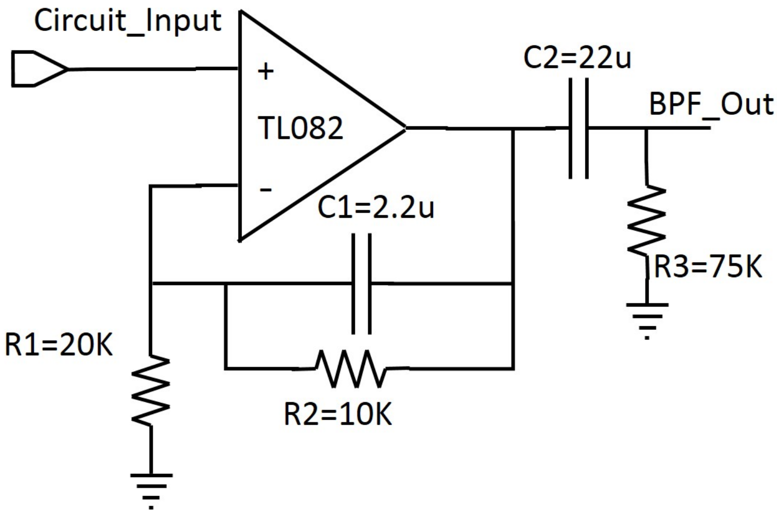

Figure 3.4. Schematics of the band-pass filter.

change in other frequency ranges. Notch filter can be designed with many different schematics and tools. In this project, it is designed using an OPAMP and discrete components. The design is shown in Figure 3.5.

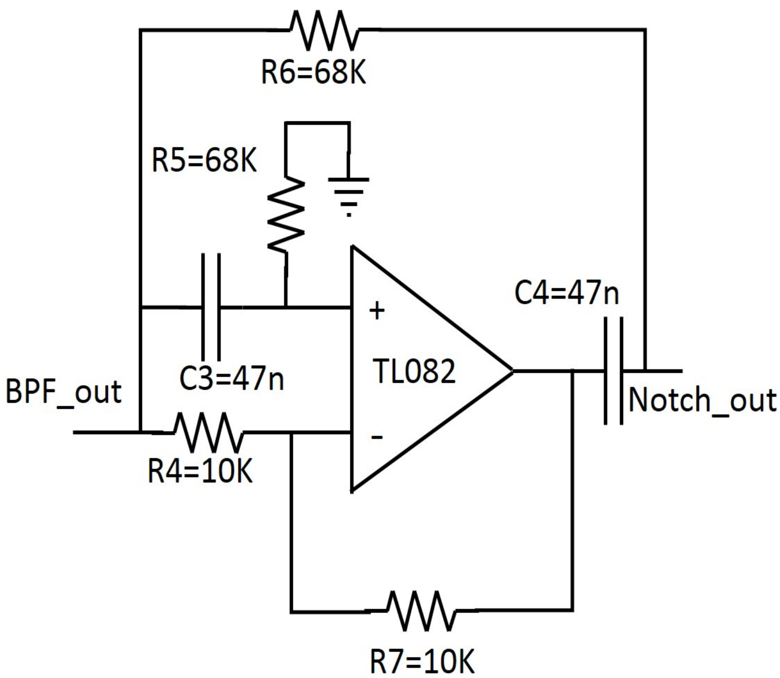

Figure 3.5. Schematics of the Notch filter.

<u>3.1.1.3. Sallen-Key Filter.</u> Sallen-Key filter is a second order active filter. This filter takes benefit of a simple design which results in smaller area. In this project, the Sallen-key filter is designed as a LPF. The schematic of a LPF Sallen-Key filter is shown in Figure 3.6. Note that R_9 and R_{11} determine the gain of the filter and make this filter the main source of providing gain for pre-amplifier stage. Gain of this circuit can be calculated as shown in Equation 3.2.

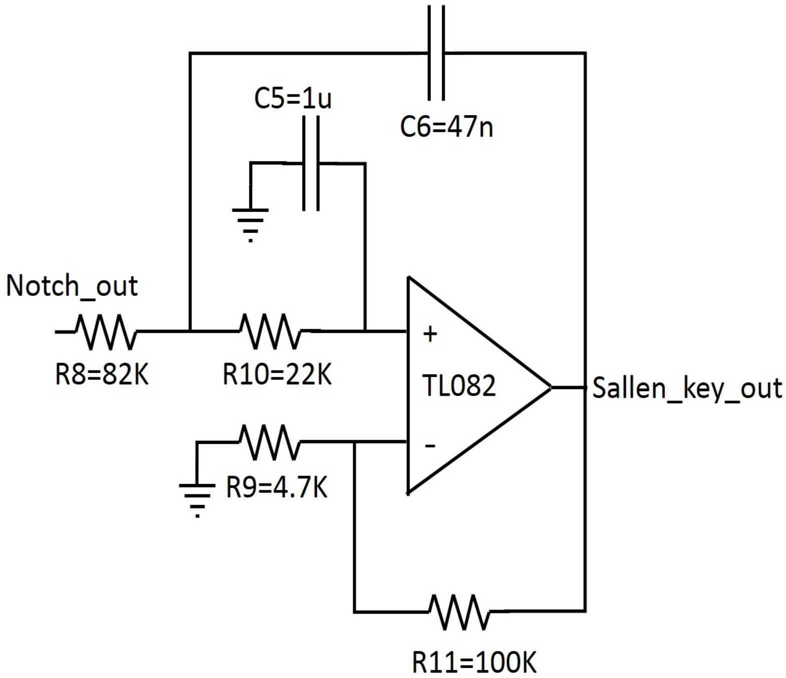

Figure 3.6. Schematics design of the Sallen-Key filter.

$$Gain = 1 + \frac{R_{11}}{R_9} \tag{3.2}$$

Writing Kirchhoff's law, the transfer function for this circuit can be calculated. Using the transfer function, natural frequency f_0 and Q factor can be extracted.

$$H(s) = \frac{1}{1 + C_5(R_{10} + R_8)S + R_8 R_{10} C_5 C_6 S^2} \tag{3.3}$$

$$\omega_0 = \frac{1}{\sqrt{R_8 R_{10} C_5 C_6}} \tag{3.4}$$

$$Q = \frac{1}{\omega_0 C_5 (R_{10} + R_8)} \tag{3.5}$$

Inserting component values according to their availability and desired frequency range in Equations 3.3 to 3.5, results in following:

$$f_0 = 17.28\ Hz, Q = 0.1 \tag{3.6}$$

However, f_0 is not the 3 dB cut-off frequency, since the filter does not have Butterworth topology. The 3 dB frequency needs to be calculated directly from the transfer function. The calculations result for Bandwidth (BW) is 4 Hz.

3.1.2. Automatic Gain Control Unit

Due to various reasons, such as changes in receiving angle, distance from radar, breathing intensity, etc, the output of the pre-amplifier stage may vary in its amplitude, which reduce the efficiency of ADC. AGC tries to keep the output level steady at a reference voltage produced inside the circuit itself. The method to maintain the signal amplitude is to manage a variable gain amplifier (VGA) with its control voltage. Control voltage is generated in a feedback loop where amplitude of the signal is sensed, stored, compared with the reference voltage and limited and control signal is generated accordingly.

3.1.2.1. Variable Gain Amplifier. THAT2181 is an operational transconductance amplifier (OTA) IC with variable gain, which is used in this design. The common method of using this IC is as presented in Figure 3.7. There are three filters in this figure, one LPF and two HPFs. C_7 and R_{12} form the first HPF. The cut-off frequency for this pair is chosen same as all other HPFs used in the analog circuit, which is 0.1 Hz. R_{15} and C_9 form a LPF with cut-off frequency of 7.23 Hz. Finally, a passive HPF consisting C_{10} and R_{16} with 0.1 Hz cut-off frequency is placed. Output of this block is connected to a buffer whose output will be the general output of the analog circuitry. In following sections the method to generate the control signal is explained.

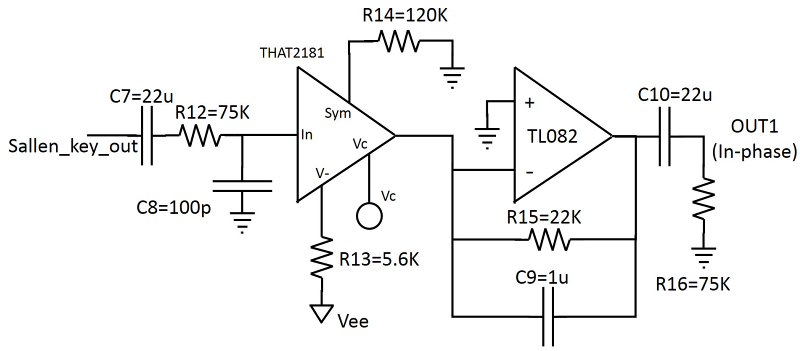

Figure 3.7. Utilizing variable gain amplifier.

3.1.2.2. Peak and Valley Detector. This block is mainly responsible for sensing and holding the output amplitude value for later use. As it is shown in Figure 3.8, positive peak is stored in top branch while negative peak is stored in the bottom one. The time constant of the RC network used in this block is chosen as same as other HPFs so that we can monitor changes in output amplitude while not changing the control signal faster than speed of human respiration. Diodes complete the peak detector circuit by not letting the capacitors discharge in wrong direction. To determine the peak-to-peak value of each of our outputs, we need to subtract them from each other (adding the absolute values). INA121 is an instrumentation amplifier that can hold this responsibility. R_{21} and R_{50} adjust the gain of each amplifier. The gain is controlled as shown in Equation 3.7.

$$Gain = 1 + \frac{50\ k\Omega}{R_G} \tag{3.7}$$

Until this part of the circuit, all the blocks were designed in pairs, for both in-phase and quadrature signals, and same is applied to peak detection block. However, to decide the control signal, both output values should be taken into account. That is why a part of the circuit is responsible to take sum of these two values. Using four resistors and an OPAMP, this can be done as well. Equations 3.8 and 3.9 illustrate the functionality of this part.

$$V_{AV} = \frac{V_{pp1} + V_{pp2}}{2} \tag{3.8}$$

$$V_o = 2 \times \frac{V_{pp1} + V_{pp2}}{2} = V_{pp1} + V_{pp2} \tag{3.9}$$

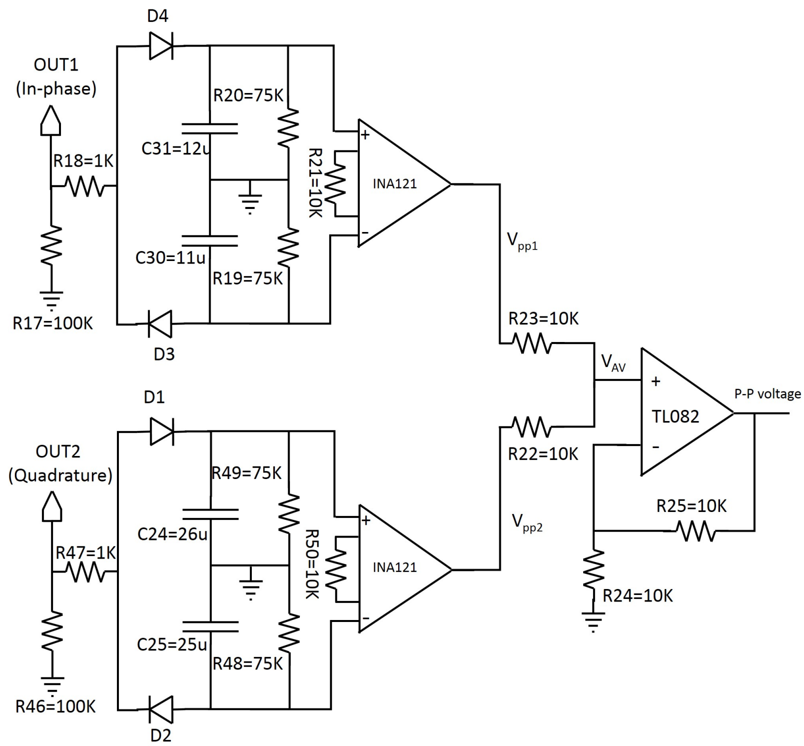

Figure 3.8. Design of the peak detector.

Now this V_o is ready to be compared with the reference voltage to generate the control signal.

<u>3.1.2.3. Generating the Control Signal.</u> Now that the output amplitude is stored, it can be compared with reference voltage. Reference voltage in this case is 2.5 V and is generated by LM385Z2.5, which is a two-terminal band-gap reference diode. First OPAMP in this block acts as the comparator. Output of this OPAMP goes to $-V_{DD}$ when signal is greater than desired value and sticks to V_{DD} when output amplitude is smaller than expected. However, THAT2181 VGA works with -0.5 to 0.5 V control voltage. As a result, a limiter is needed to keep the control signal between two mentioned values. As shown in Figure 3.9, diode D_6 and D_7 limit the control signal value

to their forward voltage which is around 0.6 volts. R_{17} and R_{28} are added to prevent non-linearities caused by sudden jumps in control voltage. They provide gain of $\frac{1}{22}$ for control voltage which reduces its maximum and minimum voltage from peak-to-peak 24 V to approximately 1 V.

VGA is extremely sensitive to its control voltage, having high frequency noise on control voltage directly affects the output amplitude and causes extra noise in the output. That is why a LPF is placed after limiter to attenuate the high frequency noises. The cut-off frequency of this added filter is 1 mHz which is lower than other LPFs in the circuit. The reason behind this low cut-off frequency is the fact that we want more stability for our system. There is a trade-off between faster system and more stable one. Choosing lower time constant for this part makes the system adapt faster to changes around it, however, every extra movement in patient, vibrations of system, passing other people in front of the package, and so on, cause abnormalities in output which does not fade away quickly, since the control signal has already changed. Higher time constant values for this part, eventually ignores short time disturbance while generating control signal, to put it in another words, sudden patient movement and other short time movements, from patient or the radar system, will have minimal effect on control signal which in turn makes it act as desired after the event is passed. Short term disturbance in time domain signal, does minimal effect on spectrum of the signal, which is calculated for long term data.

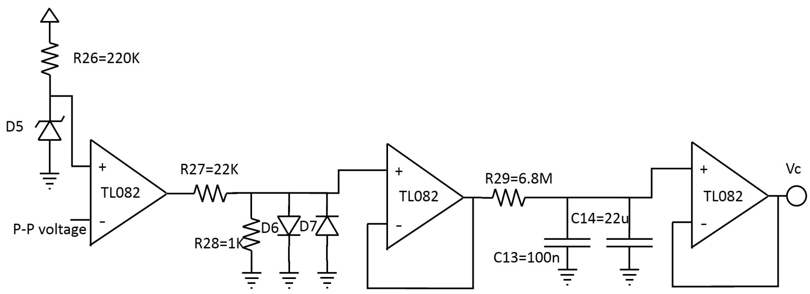

Figure 3.9. Final steps in generating control signal.

<u>3.1.2.4. Level Shifter.</u> According to chosen IC for ADC, MCP3008, the signal which is between -2.5 V and 2.5 V needs to be shifted upwards to the range 0 V to 5 V. The circuit presented in Figure 3.10 is utilized to add 2.5 V DC offset to the signal according to Equation 3.10. Finally, a LPF is added to further reduce high frequency noises in signal route.

$$V_{out} = \frac{57}{47} \times [\frac{10V_{DD}}{57} + \frac{47V_{in}}{57}] = 2.5 + V_{in} \tag{3.10}$$

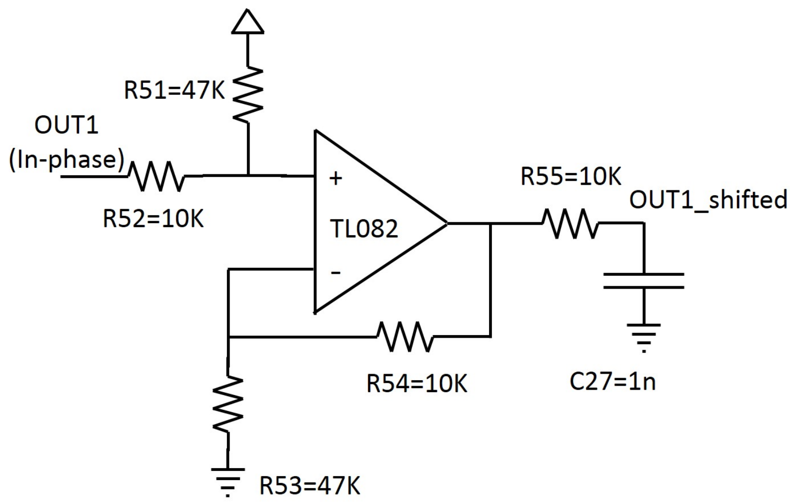

Figure 3.10. Design of the level-shifter.

At this stage, the output signal is ready to enter digital domain and be used for data extraction. Signal is limited between 0 V and 5 V. A 10 bit analog to digital converter (ADC) is used to digitize the data. The resolution of this conversion can be calculated as shown in Equation 3.11.

$$resolution = \frac{5\ V}{2^{10}} = 5\ mV \tag{3.11}$$

An ARM-based processor reads the digitized data and from this point on, digital signal processing (DSP) steps begin. Complete circuit schematic is drawn in Figure 3.11.

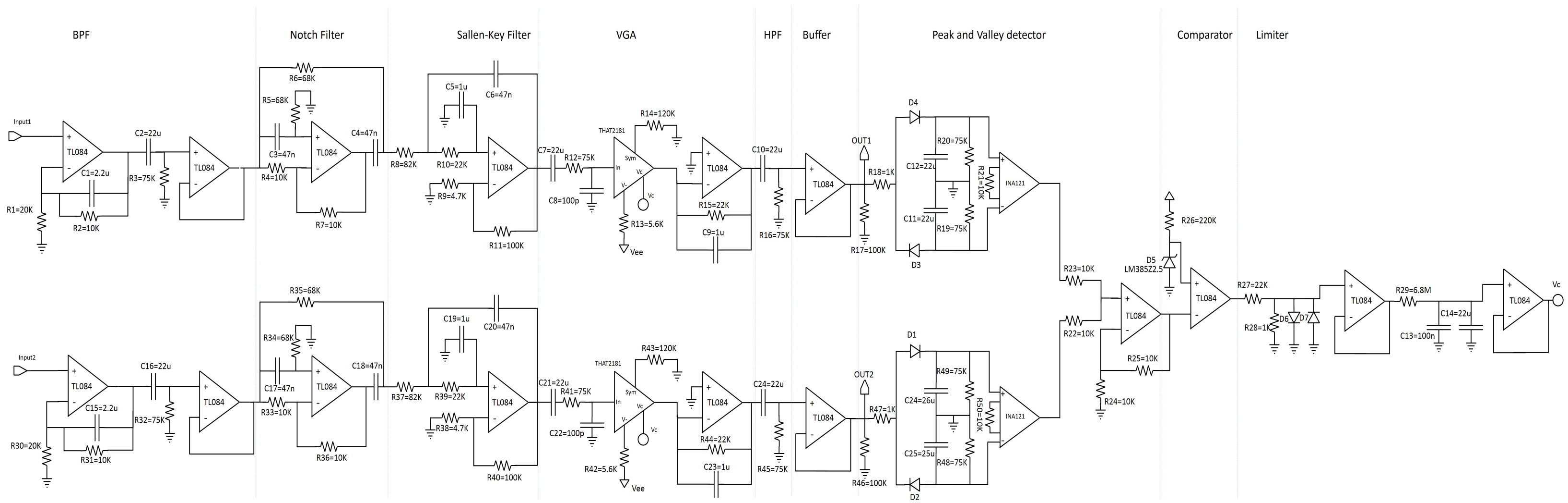

Figure 3.11. Complete analog circuit schematic.

3.2. Digital Signal Processing

3.2.1. Radar Terminal

As of this part, the signal processing is done in digital domain. Python coding language is commonly known for scientific purposes and hence chosen for this project.

According to speed of the processor, it reads the data from its general-purpose input/output (GPIO) pins. Data are read and sent via UDP through the Internet to monitoring terminal. Transmitting and receiving the data are time consuming and takes most of the CPU time and is counted as a bottleneck for speed of the code. Since most of the signal processing steps are done in monitoring terminal, Optimizing that code, can speed up the processing and as a result, we can increase the sampling rate in radar terminal. After optimization, which will be explained in next section, the radar terminal is able to send 64 samples per second. Since the maximum desired frequency is less than 32 Hz, this value obeys the Nyquist rule.

The Internet connection is required for the code to be able to send data. Code waits until Internet connection is established and then starts to work. Code detects network instabilities and waits until network stabilization and resumes sending data.

According to Equations 2.1 to 2.4, to recover relative movement, the values need to be rescaled to their former voltage level and re-biased to hover around zero value. Since in-phase and quadrature signals will be divided, their gain and scale is not of importance. However, any fluctuations in their offset change the final value. As a result, it is important to cancel the offset given to the values in ADC (while converting from [-2.5 V, +2.5 V] to [0, 2^{10}] values). For that reason, the values received in radar terminal is multiplied by 5/1024 and then reduced by 2.5.

The read data are then appended together, converted to string format, and form an array of samples that is in turn sent to a static IP assigned for the monitoring terminal and within a unique port specified for each patient. A specific time is assigned when the code is paused to get synchronized with monitoring terminal and to prevent probable loss of data.

3.2.2. Monitoring Terminal

The main tool of doing the DSPs is a code running in monitoring terminal. In general, the data are received, processed, and visualized in this part.

At first, initial steps of providing the graphical user interface (GUI) is taken. These steps include determining number of graphs and texts, as well as their dimensions and fonts. Matplotlib module is used to plot the graphs and provide the GUI.

After initial preparations, processing steps are done for each patient separately. Receiving is done in this way so that sent packages don't reach the destination at the same time and probable loss of data happens. As a result, a package of data is received from the first radar terminal, placed in an array, and converted into float format.

Nature of arctangent function forces its output to be limited between $-\pi/2$ and $+\pi/2$ range. There is an *arctan2* function that uses the sign of in-phase and quadrature signals to find the quadrant in which the result is placed and extends the range up to $-\pi$ and $+\pi$. However, there is still the need for extending this range so that in case the result get lower than $-\pi$ or higher than $+\pi$, the inevitable wrapping in the phase, gets unwrapped and relative movement can be extracted with no jumps in the signal.

The algorithm used to detect wrapping senses the jumps in the received signal. To prevent any mistakes in detecting the wrapping in the signal, 4 consecutive samples are considered and the condition in which wrapping is occurred is checked. After detecting the wrapping, the part of the signal that needs to be shifted is handled with properly so that final result looks smooth and unwrapped. Figure 3.12 shows how wrapping issue occurs when taking arctangent of a signal. The upper graph shows the desired output from the system, middle figure shows tangent of the mentioned signal and the figure beneath those, represents the arctangent of the second one. As it can be seen, the first and last figure are not similar and the last one, which we receive in monitoring terminal, needs an unwrapping to become similar to the first one.

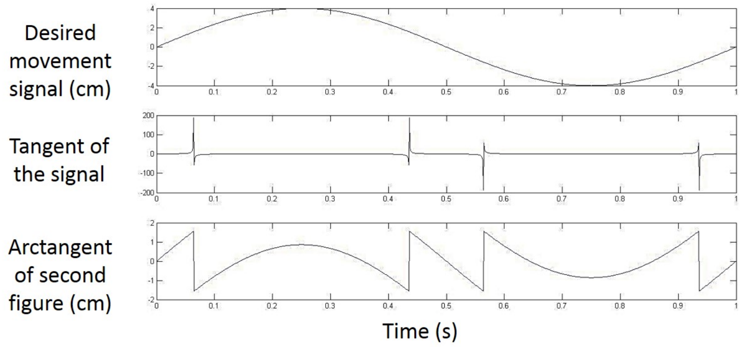

Figure 3.12. Wrapping occurs while taking arctangent.

Different sockets are defined to receive data from different ports, each corresponding to different patients. Each array of data is received from different ports corresponding to different patients. Format of the received data is in strings and needs to be converted to float which is suitable for mathematical purposes.

Now that we have the data in floating point format, mathematical operations can be done and as a result, spectrum and spectrogram of the signal can be calculated. Taking FFT of the signal and obtaining spectrum, enables us to monitor power of different frequency component in the signal. Using spectrum, average respiration rate and heart rate can be calculated. As shown in Figure 6.2, the spectrum of the signals contains important information, such as average respiration rate, heart rate, and breathing pattern (using power of respiration harmonics). FFT is taken on 90 seconds set of data with 64 sampling frequency (same as actual sampling frequency in radar terminal).

Spectrogram is also extracted in this stage. Spectrogram shows the changes in spectrum in time domain, allowing the caretaker to observe changes in patient's medical condition. Since spectrogram is time variable (inside our 90 seconds data array), Hanning window is used as a default, and each 10 seconds, spectrogram of each of the incoming signals is taken. Since sampling rate is 64 samples per second, 640 samples is chosen as number of fast Fourier transform (NFFT) and 320 samples overlapping each time.

To obtain respiration rate, most powerful frequency component in spectrum is found, ignoring DC frequency. This value represents the average breathing rate during 90 seconds of record time. This value is chosen since it is almost independent from unwanted vibrations and patient movements. However, for hazardous detection a faster approach is used which will be explained later on.

Normal respiration rates for an adult person at rest varies from 12 to 16 breaths per minute and the normal pulse for healthy adults ranges from 60 to 100 beats per minute. As a result, to find heart rate, the highest spectrum peak after third breathing harmonic is found and its frequency represents the pulse of the patient. It is due to the fact that heart rate is almost always more than three times the respiration rate.

Each time the biomedical data are calculated, the graph values are updated. There are two condition in which the warning sign alarms the caretaker of patient's hazardous condition. First when the breathing rate of the patient drop below 0.1 Hz, and second when the patient suddenly stop breathing. The second condition covers almost all of the emergency cases where the presence of a caretaker is immediately needed, since when heart fails, lungs cannot work for more than two to three seconds. But the other way around is not correct. If patient stops breathing, heart still can pump up the blood in veins and use the remaining oxygen in blood and can work up to a minute. Those are the reasons why detecting breathing failure is sufficient and enough as a warning.

Images showing danger detection is shown in Chapter 7.

The designed GUI is presented in Figure 3.13. There are 9 graphs placed in columns of 3 graphs, each representing different patient. For each column, upper graph shows the relative movement of the patient's chest in time domain, second one shows spectrum of that movement and the one below others show spectrogram of the signal. Spectrogram shows changes in spectrum through time. Normally, changes in the frequency of the dominant signal, which is first harmonic of respiration, is visible in this figure.

There is a status sign placed below each column corresponding general condition of the patient, in case the code detects abnormalities in patient's medical condition, the warning alarm will be shown on the screen, informing the caretaker of the situation.

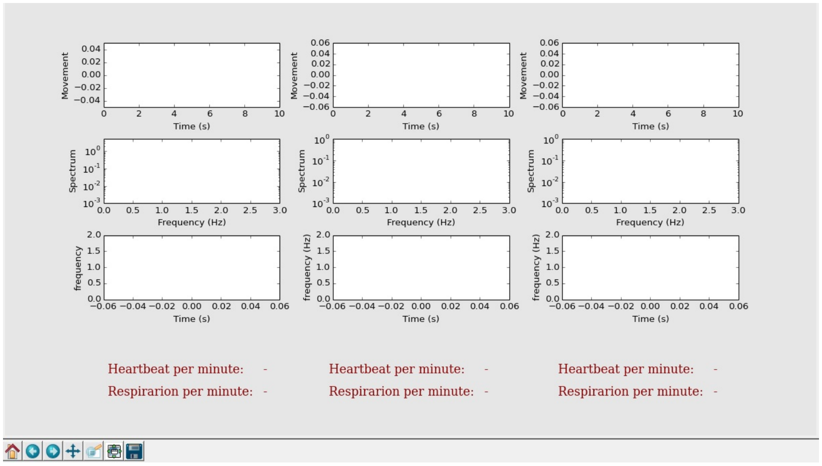

Figure 3.13. Graphical User Interface.

Finally, to hold the record of the medical conditions of a patient, the data are stored in files for using later on in different ways and various algorithms. For instance, many useful information can be extracted from breathing pattern, frequency, and stability of a patient. These information does not necessarily need to be gathered real-time, they can be accessed and used later on by a doctor.

A MATLAB code is written to utilize the saved data and use it for illness diagnosis. In this code, some extra information is extracted form the data such as, maximum and minimum of respiration and heart rate, as well as an instantaneous breathing rate graph. Any disorder observed in the data extracted in this code, can be used to find any probable respiration disorder and some other illnesses.

This code provides the GUI presented in Figure 3.14 which makes it easy to use and monitor the data as well as giving some tools to work with, such as pan, zoom, and save. Some tools, such as pan, zoom, and save is provided for user and can be utilized for careful data observation.

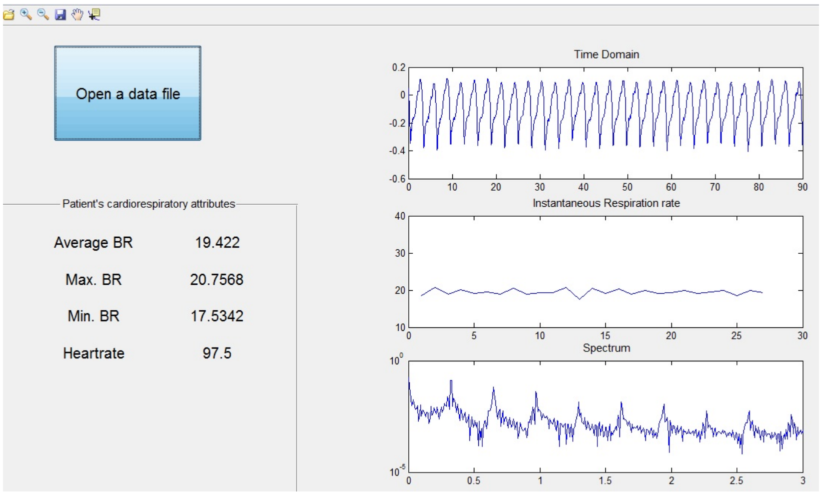

Figure 3.14. Graphical user interface provided for illness diagnosis.

Information such as average, minimum, and maximum of breathing rate as well as average heart rate is presented in this code. User, which is usually the caretaker, opens a desired data file each time and monitors the patient's condition.

Almost all diseases have some indicators, and many of them affect respiration rate. Abnormal respiration rate and also variations in respiration rate can be accounted as signs of an illness. Usually respiration get affected sooner than other life signs, that is why monitoring it can prevent further damage to patient's body in case of an illness.

Respiratory rate performs at least as accurately in identifying patients at risk of these adverse events as pulse rate and the systolic blood pressure. In fact, abnormal respiratory rate is one of the best independent predictors of cardiac arrest.

Changes in the severity of chronic illnesses such as chronic obstructive pulmonary disease (COPD), congestive heart failure (CHF), Arthritis, Asthma, Cancer, Diabetes and HIV/AIDS can be detected using respiratory rate monitor [15].

A typical respiratory rate (RR) can be between 12 and 20 per minute for adults [16]. However, many factors aside from physical activities can change this number. For instance, airway obstructions like asthma, emphysema and COPD will increase respiration rate causing tachypnea (RR $>$ 30) [17]. The importance of respiration monitoring can be understood from mentioned examples [15].

4. PACKAGING AND HEALTH-CARE NETWORK

To realize the idea, a proper packaging had to be designed that could hold all the boards and have an acceptable look. The designed circuit board is a 10.3 cm by 7.7 cm rectangle. The dimensions evolved though time and different prototypes. First prototypes had around 20 cm by 14 cm size and was fabricated using through-hole lumped elements. Final version of the circuit however, is built using surface-mount devices (SMD) with slightly lower tolerance for more robustness and precision. The radar circuit is shown in Figure 4.1. Aside from main circuit parts, when packaging is

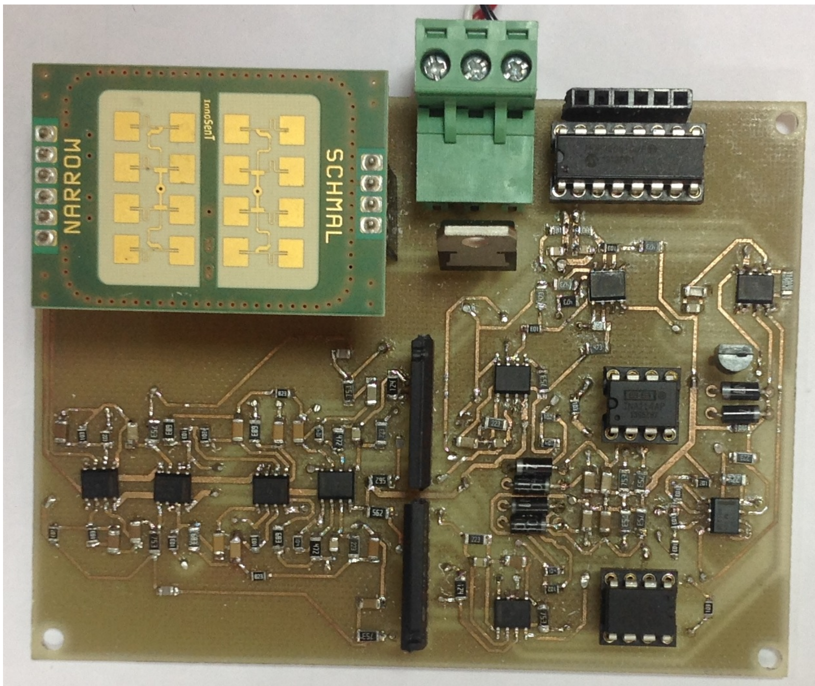

Figure 4.1. Fabricated interface for sensor signal filtering and amplification.

proposed, there is a need for power supply circuit that can smoothly provide power for all circuits. In this case, a ±12 volts power supply plus a ground is needed for the radar circuit. A +5 V is needed for ARM-based processor, which works as data acquisition. The radar circuit consumes around 110 mA current which can be handled with voltage generators and regulators. However, the processor needs more current, up to 300 mA and as a result, a special 5 V voltage generator, which is a custom circuit is used and placed inside the power supply circuit. The fabricated power supply board is shown in Figure 4.4.

The simplified block diagram of the power circuit is shown in Figure 4.3. ICL7662 is a CMOS voltage converter that is used to generate -12 V for radar circuit. Output voltage of the ICL IC drops as its load current increases, as shown in Figure 4.2, two of them are placed in parallel with each other to make the load half as well the voltage drop.

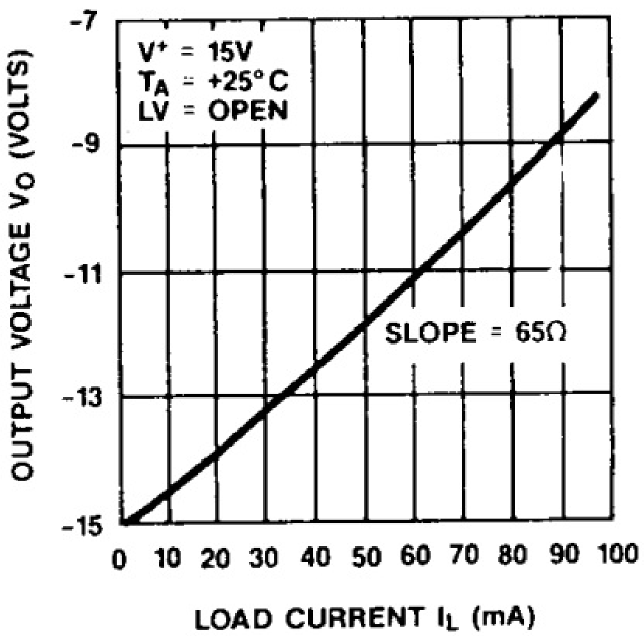

Figure 4.2. ICL7662 output voltage vs its load current [18].

LM7912 is a -12 V voltage regulator used to ensure consistency and smoothness of the voltage fed to the radar circuit. LM7812 is used to provide +12 V supply voltage.

The circuit input comes from a 19 V, 1 A adapter. Diodes are placed in the entrance of the circuit to absorb 1 V and prevent overheating of ICLs. The 5 V voltage regulator is a custom circuit, commercially available, and able to derive enough current for our ARM-based processor. The outputs of the circuit, V_{cc} and V_{ee}, are +12 and -12 V supply voltages respectively for the radar circuit.

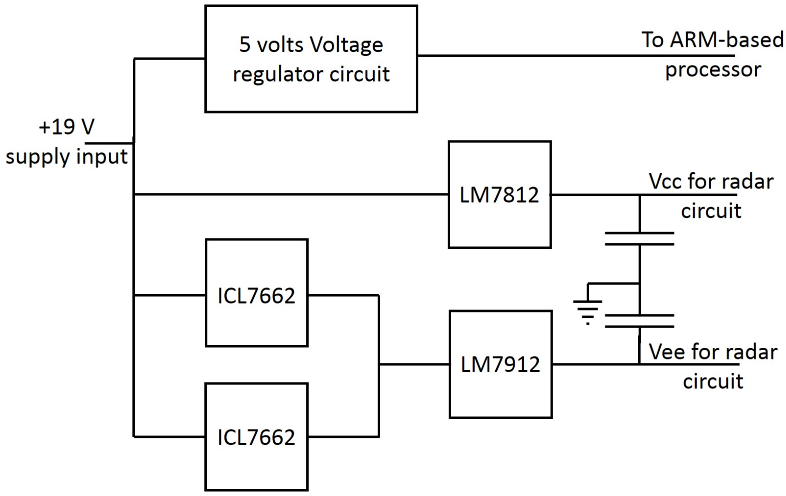

Figure 4.3. Simplified block diagram of the power supply circuit.

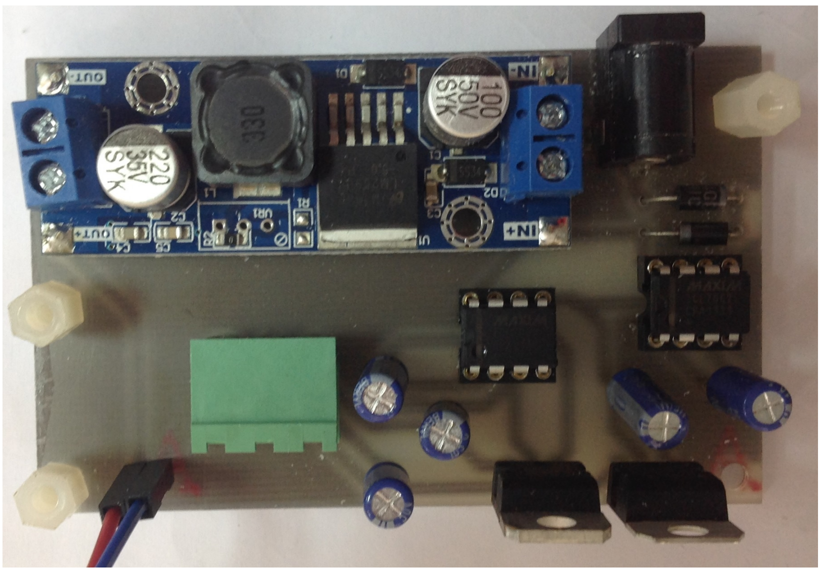

Figure 4.4. Fabricated circuit to supply power to all other circuits.

The designed power circuit has dimensions of 5 cm by 8 cm. The used ARM-based processor has 8.7 cm by 5.8 cm area. Different facts are considered for placing the boards and deciding a size for the package itself. These considerations, such as output and input ports, which include power jack and local area network (LAN) cable, sensor position in final package, and routing inside the package, are aimed to decrease the dimensions and leave the performance untouched and look as neat as possible. The final packaged system is shown in Figure 4.5. The whole package takes 19 cm by

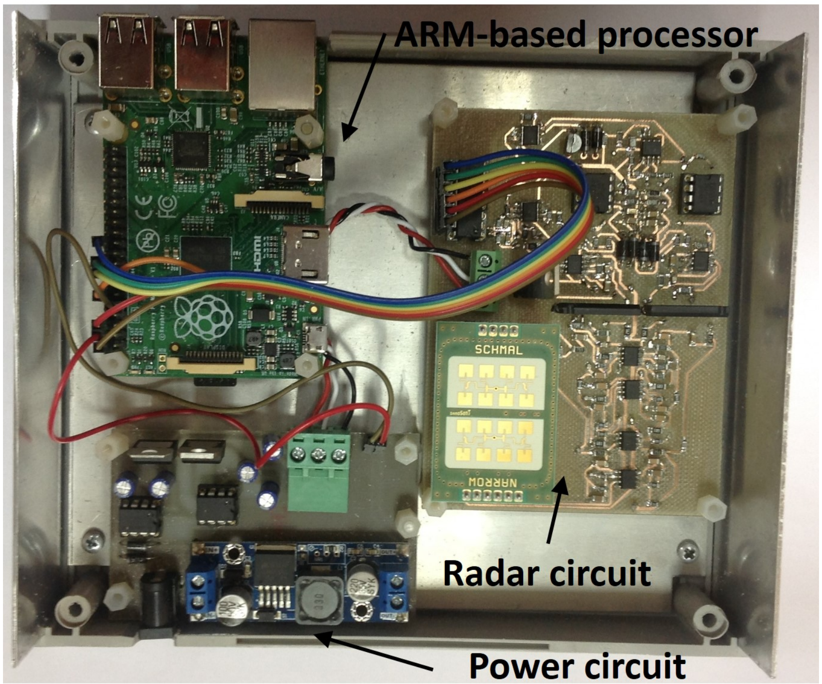

Figure 4.5. Inside view of the final package.

15.5 cm by 5.5 cm space and is placed inside a holder (Figure 4.6) for measurements.

Next step was to further expand the system functionality. It was decided to make 3 copies of every circuit and put them in different places over different patients. Thus, three radar circuits, ARM-based processors, power supply circuits, mechanical holders, and so on, are fabricated. They are placed in different rooms with access to the Internet.

These three stations are connected to the same monitoring terminal, which plays the server role in this network. It gathers all data and monitors all patients.

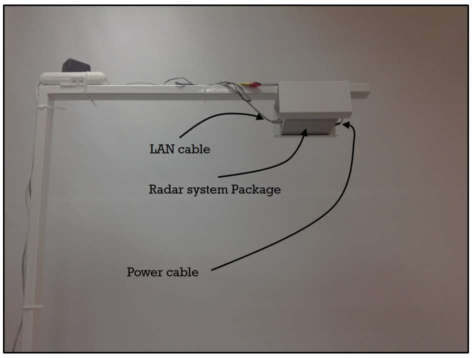

Figure 4.6. The mechanical tool fabricated to hold each sensor above the sleeping patient.

5. SIMULATION RESULTS

Transient and AC simulations are performed for each block of the circuit individually and in cooperation with other blocks to check functionality and optimize the performance. Simulations are done in computer aided design (CAD) tools such as Hspice, LTspice, MATLAB, Pspice, and printed circuit boards (PCB) are fabricated with LPKF PCB fabrication tool.

5.1. Pre-amplifier

As mentioned in previous chapters, the circuit is designed to filter out frequencies beneath 0.1 Hz and higher than 7 Hz and generally act as a low noise amplifier (LNA). We also aim to neglect 50 Hz noise as much as possible. Simulation results for each block is shown in Figures 5.1 to 5.3.

The simulation result for whole pre-amplifier stage is shown in Figure 5.4

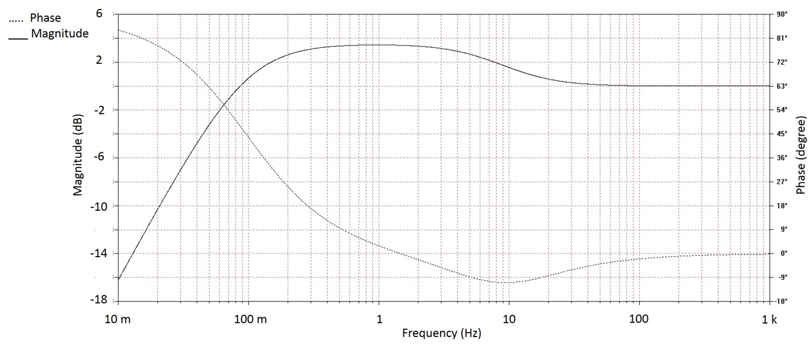

Figure 5.1. AC response of the BPF.

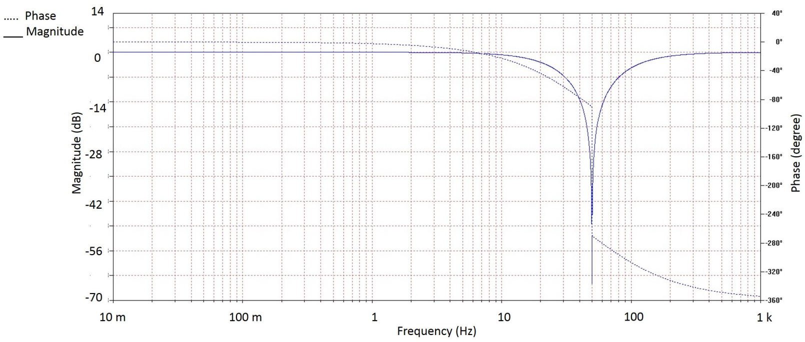

Figure 5.2. AC response of the Notch filter.

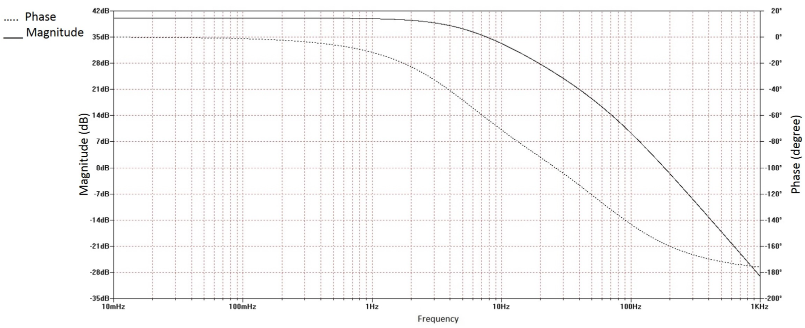

Figure 5.3. AC response of the Sallen-Key filter.

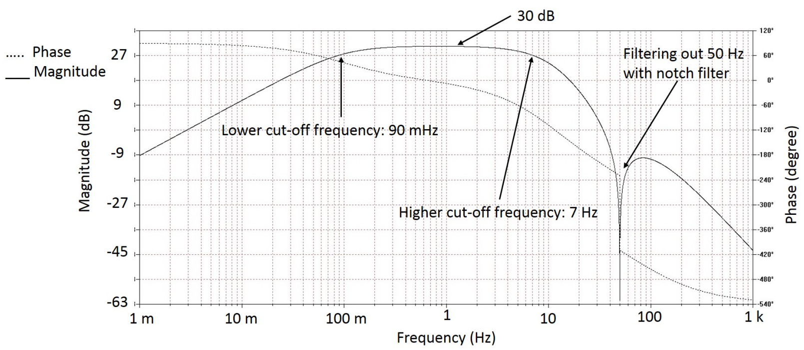

Figure 5.4. AC response of the pre-amplifier stage.

5.2. Automatic Gain Control

AGC has a dynamic functionality and AC simulations normally cannot be used to test the performance of the circuit. That is the reason why the simulation for AGC block is done in transient domain.

The main part of this block is the VGA which has the variable gain according to its control voltage. THAT2181 IC is chosen for this part and the changes in its gain relative to its control voltage can be seen in Figures 5.5 and 5.6.

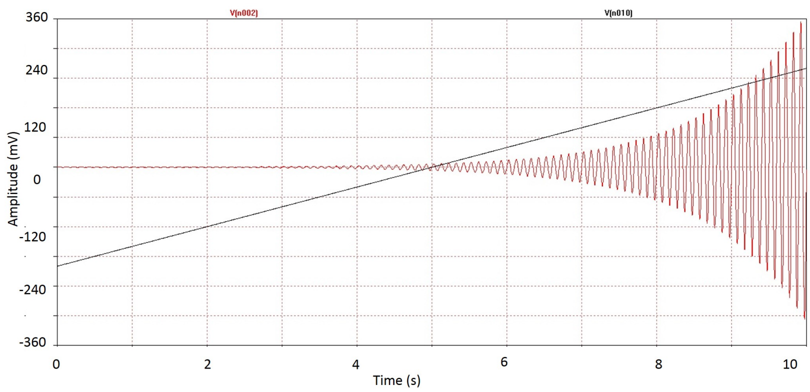

Figure 5.5. Gain of THAT2181 increases as its control voltage increases [19]. Red line is the output of the amplifier and black line is the control voltage.

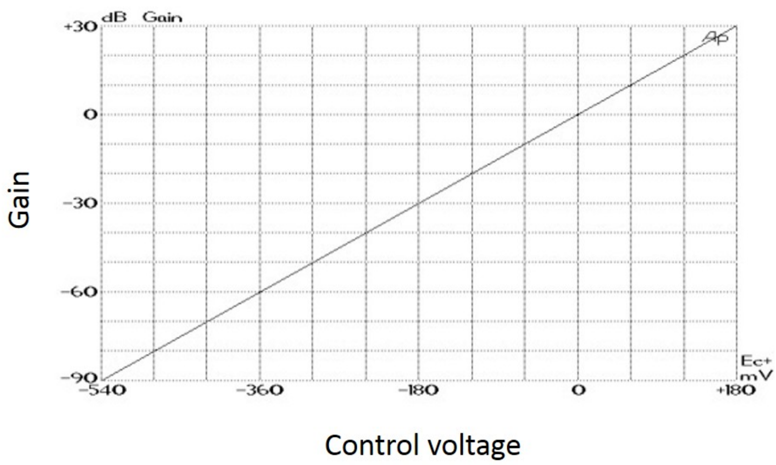

Figure 5.6. THAT2181 gain vs control voltage.

When used with RC networks in input and output stage, THAT2181 works as filter. The output of the IC with constant control voltage is shown in Figure 5.7.

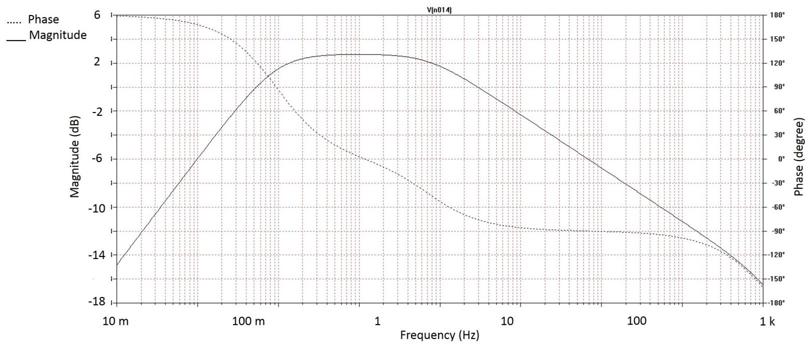

Figure 5.7. AC output of THAT2181 IC, note the 0.1 Hz and 7 Hz cut-off frequencies.

The designed peak and valley detector works as shown in Figure 5.8. Note that absolute values of peak and valley of the signal are added together and multiplied by some gain. The jumps in the signal will not affect the control signal since they will be filtered later on in the circuit.

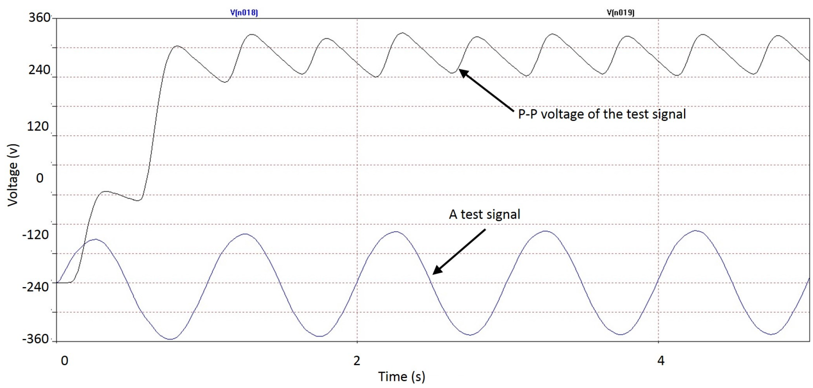

Figure 5.8. An example of functionality of peak detector circuitry.

The output signal in Figure 5.8 needs to be compared with reference voltage and limited to be suitable as a control signal for THAT2181. A comparator plus two limiter diodes are responsible for this matter and as Figure 5.9 shows, they can limit the signal to maximum of V_{fm} of the diode. In this case, since the peak-to-peak voltage is less than 5 V, the control signal is set to maximum, which is 0.4 V in this case.

To simulate previously mentioned blocks in AGC part altogether, transient simulation is needed, since concept of gain control is only rational in time domain. An

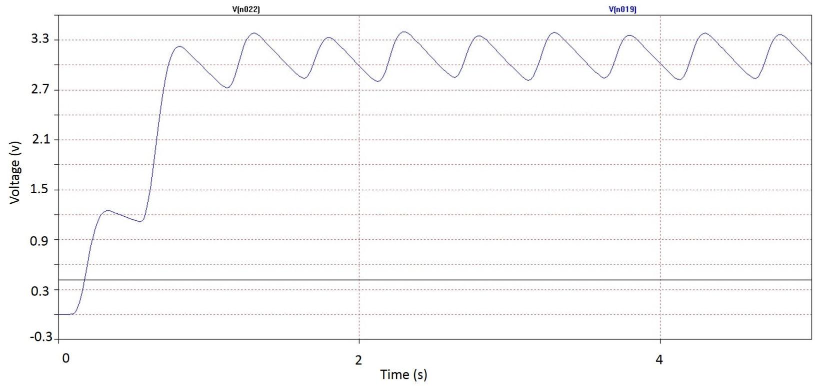

Figure 5.9. Peak-to-peak voltage is compared to reference voltage (5 V) and limited between -V_{fm} and +V_{fm}.

input is chosen that changes at one point in DC offset, frequency, and amplitude to test capability of the AGC to adjust to all kinds of changes that might happen in its input signal. This is a good way of approximately find the settling time of the circuit. However, this case will never happen and all the time changes in the sensor outputs is much smaller than assumed here. That is why in reality, the settling time of the system while responding to changes in its surroundings and especially in its field of view is at most 30 to 40 seconds.

The input to the circuit and its output is shown in Figures 5.10 and 5.11.

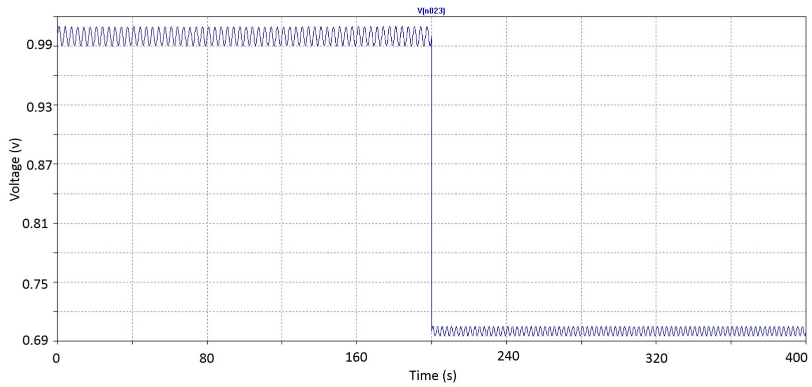

Figure 5.10. Input signal applied to the AGC.

After the situation changes in front of the radar circuit, such as the time when patient changes, returns to his/her place, and other changes, the circuit takes around

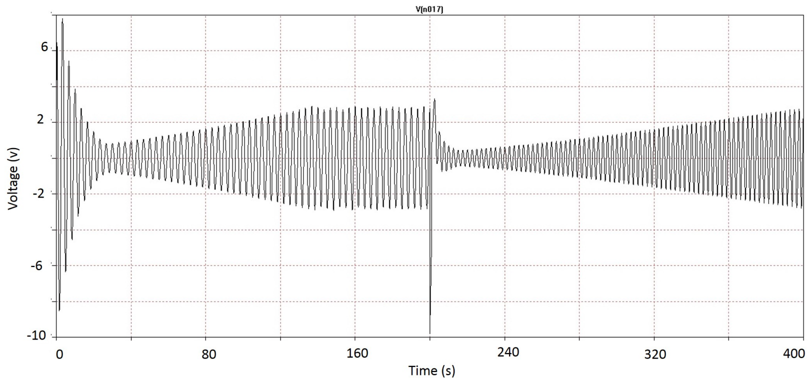

Figure 5.11. Transient output response of the AGC.

100 seconds to adapt with new conditions. However, since the channels finally will be divided together, what is seen in monitoring terminal is usually less than 30 seconds settling time. The startup time for circuit is usually less than time required for the ARM-based processor to boot.

6. RADAR CIRCUIT ELECTRICAL CHARACTERISTICS

The fabricated radar circuit is tested so that its functionality get approved and its performance measured. To test the radar circuit, it is placed in front of the mechanical periodic respiration simulator, then a patient is placed in front of the radar. The result for both of these conditions is presented in Figures 6.1 and 6.2.

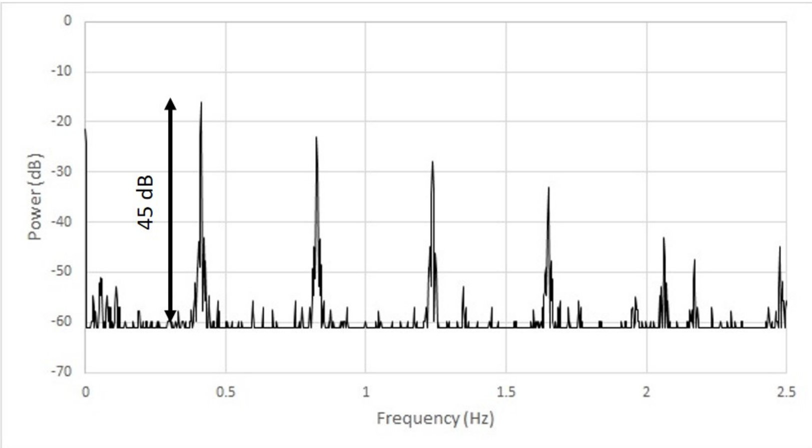

Figure 6.1. Radar circuit output while sensor is placed in front of the mechanical respiration simulator.

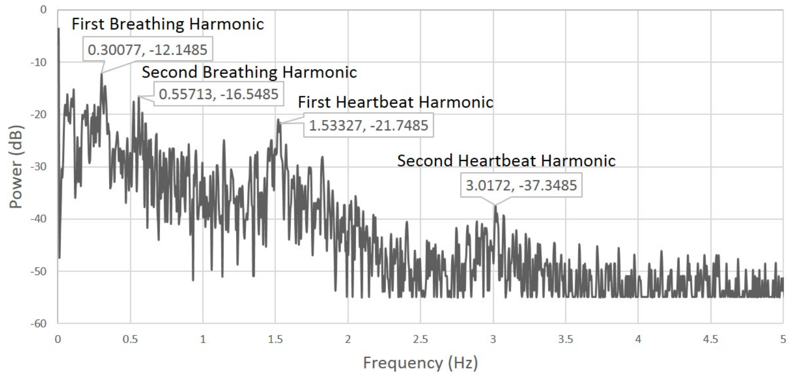

Figure 6.2. Radar circuit output while sensor is placed in front of a human.

The difference between two figures represents the noise human movements add to the signal the circuit receives. There are many tiny vibrations on our body surface which will be recorded by this system.

Also Figure 6.1 shows the signal power is almost 45 dB greater than noise power, which is far more enough than the required quality to detect heart beats. Considering this is output noise, we know input referred noise will be much lower since the sensor interface amplifies the signal throughout the signal path. However, the bottleneck for the noise floor of the whole system would be ADC. Since the used ADC is 10 bit ADC, minimum voltage detectable would be $5/2^{10}$ which is around 5 mV. This number still satisfies the minimum sensitivity to detect heartbeats.

Ideal sensor interface circuit would be the one which does not affect the frequency spectrum of the signal and does not add distortion. To put it simply, it should not add harmonics, or move the main frequency. To test the effects of the circuit itself on the signal, the sensor is removed and the radar is exposed to pure sinusoidal input as well as a pulse train signal and the output for each case is observed.

The output of the circuit to sinusoidal input is compared with a pure sinusoidal signal with same amplitude. This way, the non-linearities that is added to the signal can be seen. It should be noted that in continuous time, the FFT of the sinusoidal signal would be an impulse in the frequency of the mentioned signal. However, the measurement equipment have a sampling rate which distort the signal. That is why the pure sinusoidal signal is also sampled with same sampling rate to be in same condition as the circuit output.

The pure sinusoidal signal altogether with the radar circuit output to the sinusoidal input in frequency domain is shown in Figures 6.3. The plotting frequency range is chosen after the main harmonics to check for probable additional harmonics. the circuit output to a pulse train input is shown in Figure 6.4. Some of the most important electrical characteristics of the radar circuit in its steady state is measured and gathered in Table 6.1.

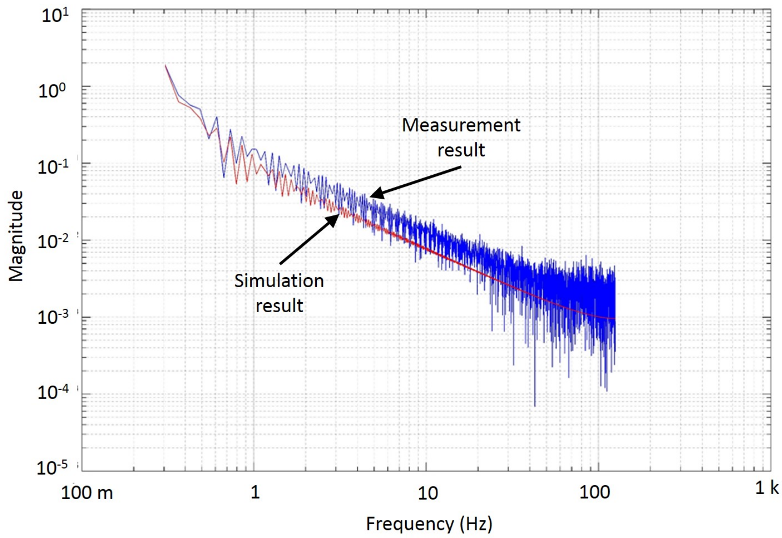

Figure 6.3. Radar circuit output response to a sinusoidal input in AC mode in comparison with the pure sinusoidal.

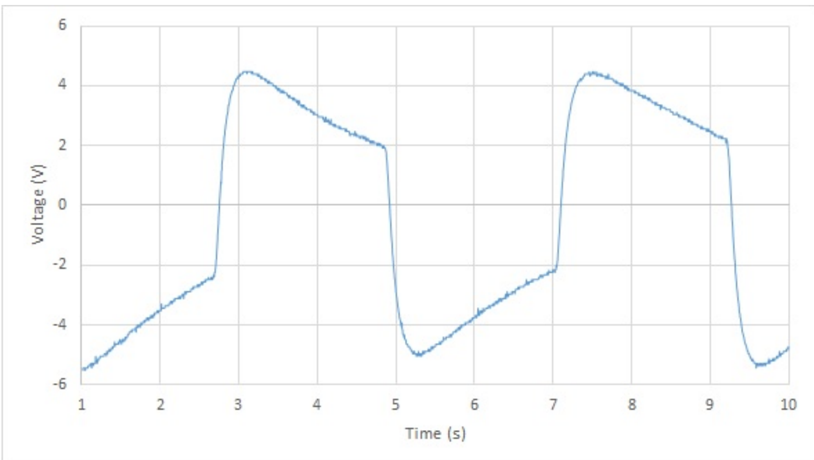

Figure 6.4. Radar circuit output response, where a square wave test signal is applied to the input of the analog circuit.

Table 6.1. Electrical characteristics of the radar circuit in steady state.

Parameter	Symbol	Condition	Min.	Typ.	Max.	Units
Supply current	I_{cc}	with sensor	111	112	113	mA
		without sensor	66	68	70	mA
Supply voltage	V_{cc}	-	10	12	12	V
Lower cut-off frequency	F_L	-	-	240	-	mHz
Higher cut-off frequency	F_H	-	-	7	-	Hz
Gain	A_V	$V_c = 0.2mV$	-	61	-	dB
		$V_c = 0$	-	31	-	dB
		$V_c = -0.2mV$	-	0	-	dB
Fundamental signal to noise floor ratio	SNR	-	-	> 45	-	dB

7. MEASUREMENTS

7.1. Measurement Setup

Verification of functionality of the system is only possible if the system output is compared with a trusted traditional measurement method. For this reason, the proposed system is tested simultaneously with a traditional respiratory and heart rate measurement tools. Biopac MP30B-CE device is chosen for this purpose with a respiratory measurement belt and contacts for ECG. The measurement setup would be as illustrated in Figure 7.1.

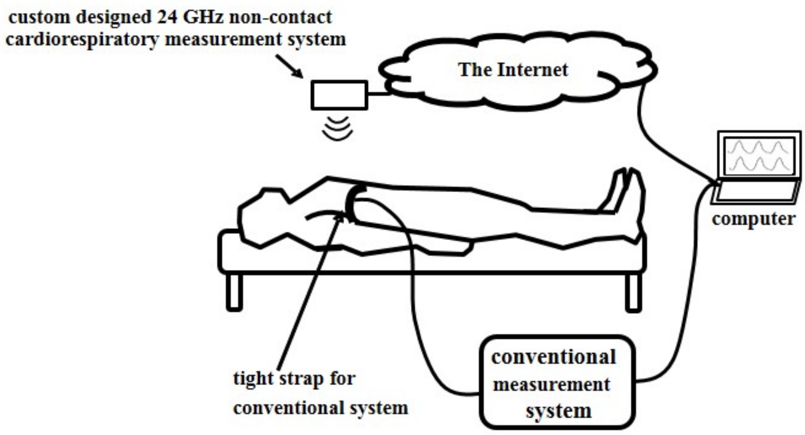

Figure 7.1. Measurement setup to test accuracy of the proposed system.

To fully test the capabilities of the system, it is tested in different conditions. Variable environmental conditions include different patient rotation while sleeping, different distances, different positions under the radar, and so on. The best result is expected when the patient's chest is exactly under the radar, where the chest surface will be perpendicular to the incoming waves. The system is also tested from behind a thin barrier, since this may be the case for some patients (early born infants for instance).

To have a better understanding of the circuit functionality, two mechanical respiration simulators are built. These respiration simulators, produce a periodic movement with controllable frequency. As a result, it can recreate a perfect breathing pattern which can be detected by our radar system. These simulators does not have extra vibrations that we can see on human chest surface. So, it helps us to monitor the response of the system to a perfect input movements and shows how much extra body movements affect the final spectrum.

The mechanical respiratory simulator is fabricated based on a motor that using generated movements, lifts a metallic plate periodically, creating a model of human chest movements stemmed from respiration (Figure 7.2).

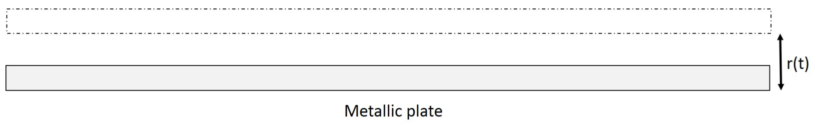

Figure 7.2. mechanical respiratory simulator movements.

One of the mechanical simulators is shown in Figure 7.3. For each condition,

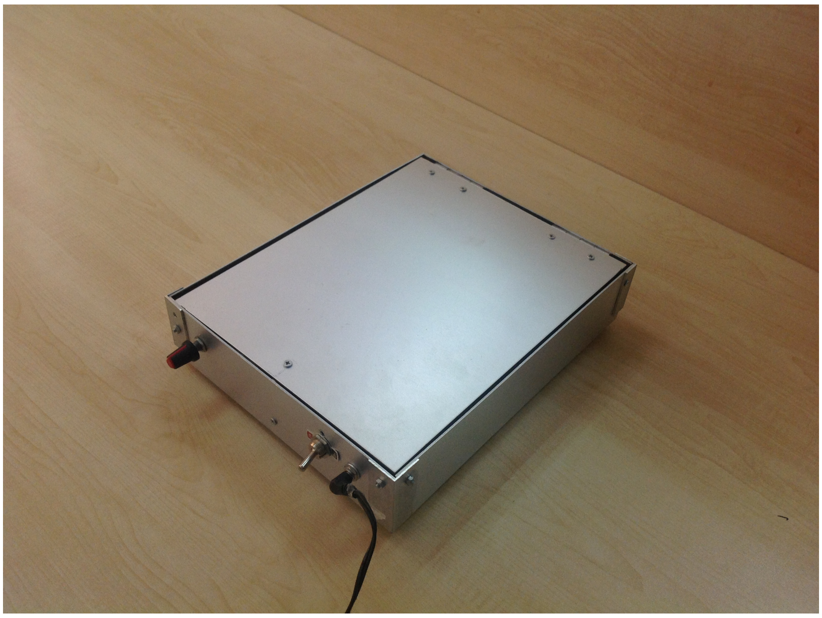

Figure 7.3. Image of the mechanical simulator.

the test result is presented for both the proposed radar system and the traditional measurement tools.

In the first set of measurements, the aim to see if the fabricated system generates the vital signs with an acceptable error rate comparing with the reference measurement. As a result, two of the systems are placed over two mechanical respiratory simulators, while third one is detecting respiration and heart rate of a person, who is also being monitored with traditional measurement tools, Figure 7.1.

7.2. Measurement Results

In following reference measurement results, for each case, the Biopac (company that manufactured the reference device in use, which also is the name the software used to connect the computer to the device) can be used to extract instantaneous heart rate and respiratory rate, however in some cases, the software is unable to do so and the actual value of those parameters can be found by counting the peaks in corresponding graph in reference figure.

The designed GUI shows medical conditions of three patients, each represented in a column and as described in Figure 7.4

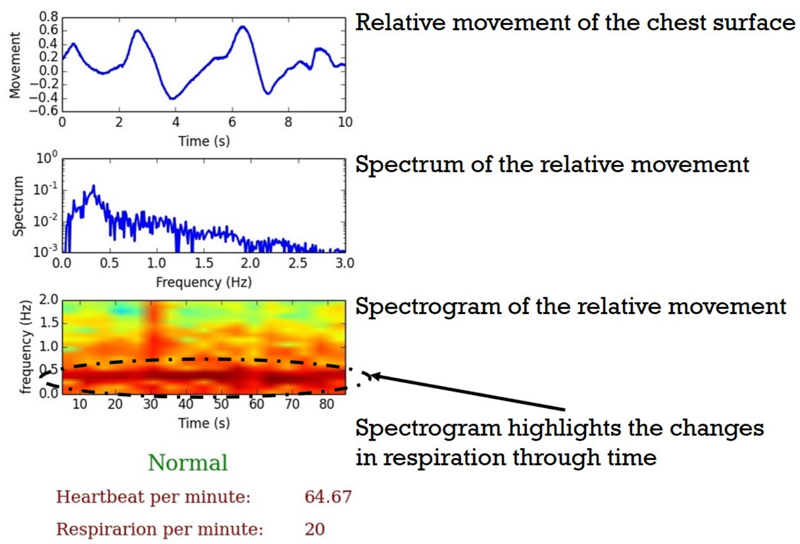

Figure 7.4. Explanation of GUI graphs.

First, the distance between the device and person is chosen as 1 meter and the patient is sleeping faced to the device. Results are shown in Figures 7.5a and 7.5b. The reference measurement shows 89 beats per minute (BPM) and our proposed radar circuit is showing 80 BPM. In case of the respiration rate, the reference measurement indicates on 21.1 while the radar system calculated that one as 22 respiration per minute.

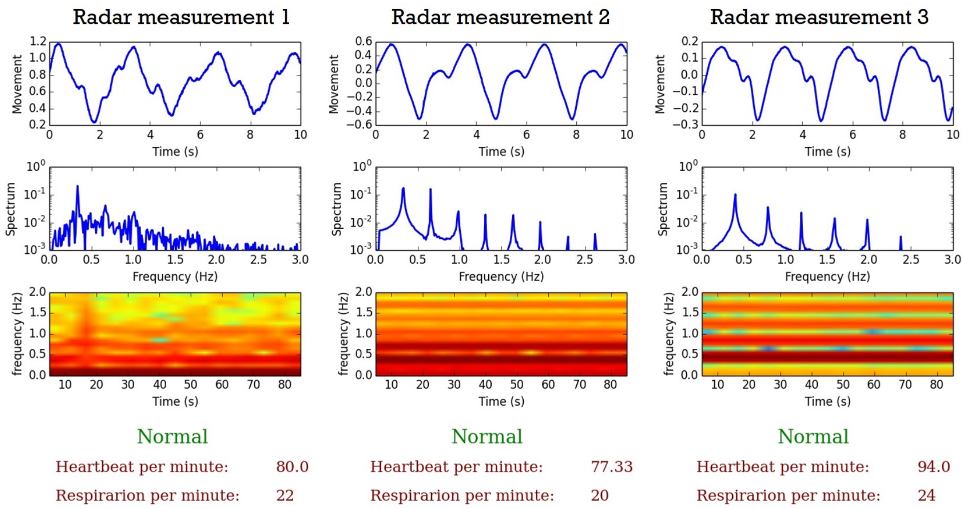

(a) Result of the proposed radar circuit.

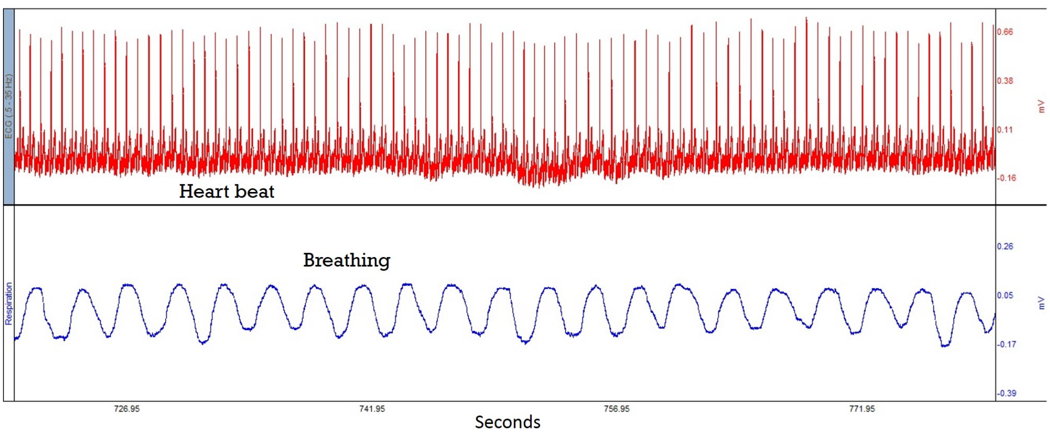

(b) Result of the reference device.

Figure 7.5. Measurement result for when radar system is placed in 1 meter distance from patient viewing front of him, 2^{nd} and 3^{rd} radar systems are watching mechanical simulators.

For next test, the patient is rotated by 90° so as if he is sleeping on his side. The distance is still 1 meter and no barrier is placed between radar and patient. The result is gathered in Figure 7.6. For this case, as the reference tool indicates, the heart rate varies between 60 BPM and 85 BPM, and our radar system shows 69.33 BPM. Respiration rate is shown 19.3 in our system, however there are 20 breaths done in one minute actually.

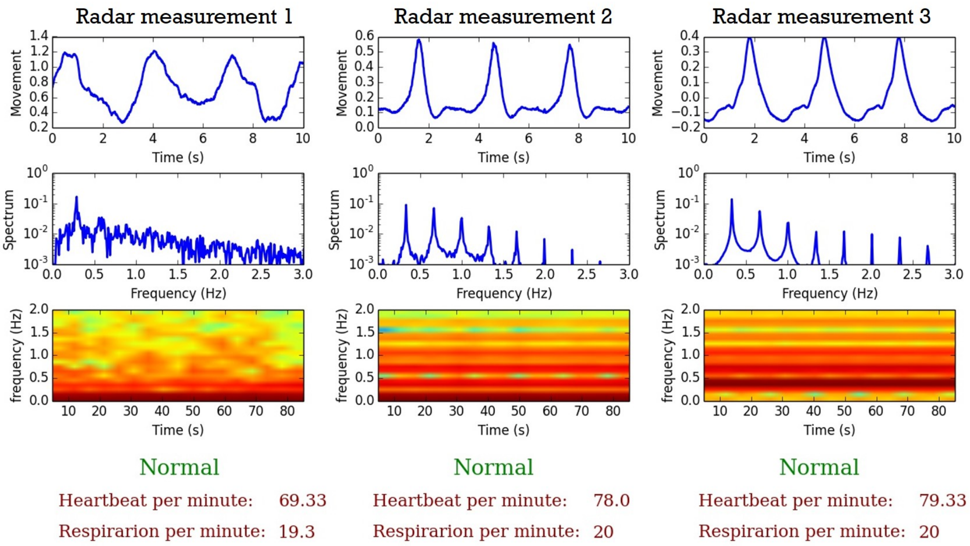

(a) Result of the proposed radar circuit.

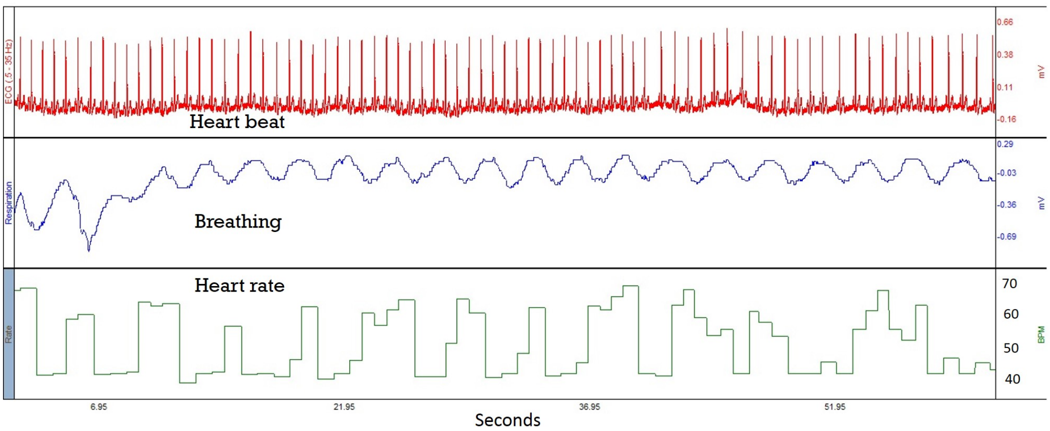

(b) Result of the reference device.

Figure 7.6. Measurement result for when radar system is placed in 1 meter distance from patient viewing his side of body, 2^{nd} and 3^{rd} radar systems are watching mechanical simulators.

Then with same distance, patient is sleeping on his stomach and the results are recorded. This gives the most stable result of all since human back moves almost identical on each respiration and on each heartbeat. Heart rate varies between 60 and 92 according to reference tool and our system shows average heart rate of 74.67, respiration rates are shown 21 and 19.7 respectively.

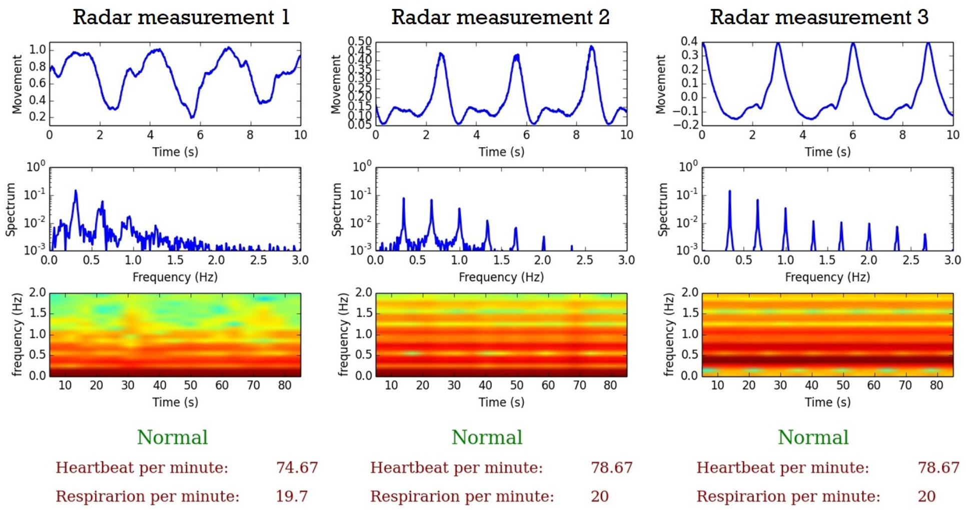

(a) Result of the proposed radar circuit.

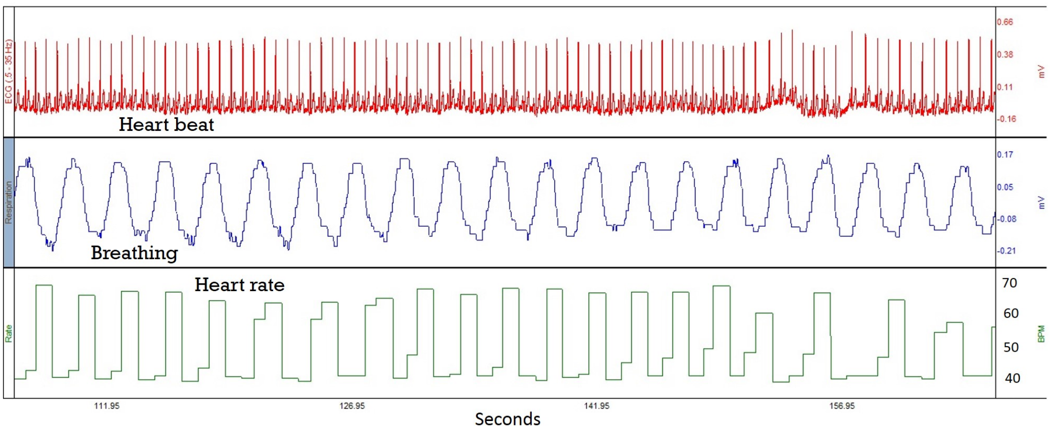

(b) Result of the reference device.

Figure 7.7. Measurement result for when radar system is placed in 1 meter distance from patient viewing his back, 2^{nd} and 3^{rd} radar systems are watching mechanical simulators.

This time, distance is increased to 2 meters and radar is viewing front of the patient. This time reference measurement shows 20.5 RPM and 40 to 68 BPM, however, the radar circuit shows 22 and 64.67 respectively.

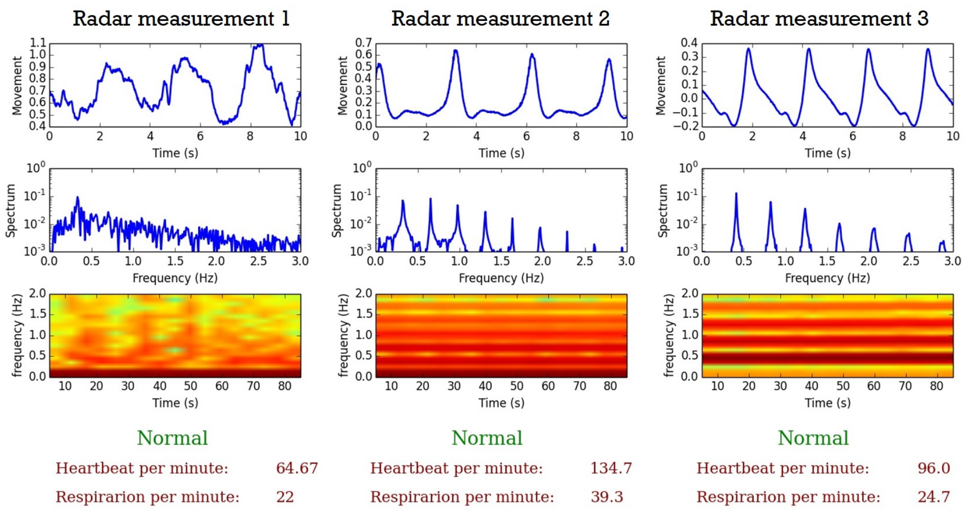

(a) Result of the proposed radar circuit.

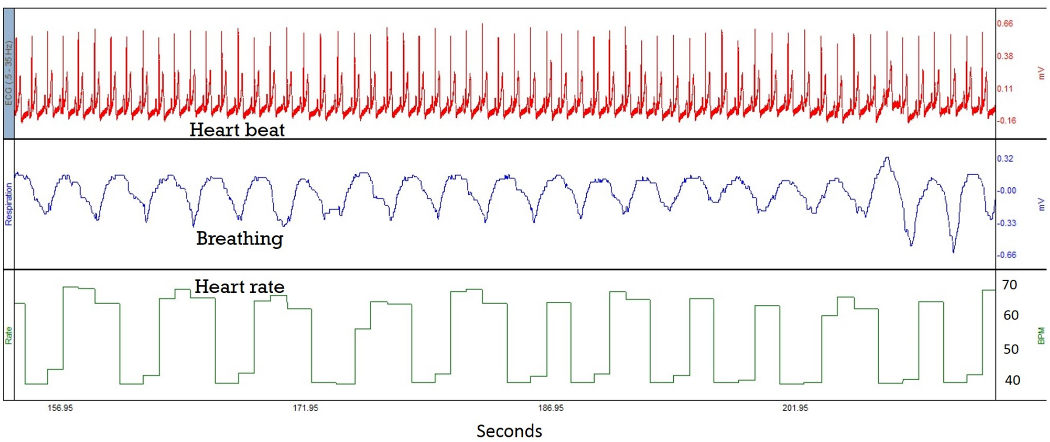

(b) Result of the reference device.

Figure 7.8. Measurement result for when radar system is placed in 2 meters distance from patient viewing front of him, 2^{nd} and 3^{rd} radar systems are watching mechanical simulators.

Now it is time to test the functionality of the system to detect hazardous situations. For this case, there are two possible conditions to trigger the warning system. First, a human can lay down under a system and stop breathing for 5 to 10 seconds. Second, a mechanical respiratory simulator can be used and stopped to check the mentioned feature. First option does not generate the similar conditions of a dangerous situation, since the patients still has heartbeat and also while holding his breath, his body makes more random movements which makes it look like a human is still lying under the radar system, moving. However, first option is selected to test the functionality of the system on humans, Figure 7.9. In this case, the patient is asked to hold his breath for 6 seconds. Although his body makes more vibrations than normal, the system detects the lack of strong respiration and sets off the alarm.

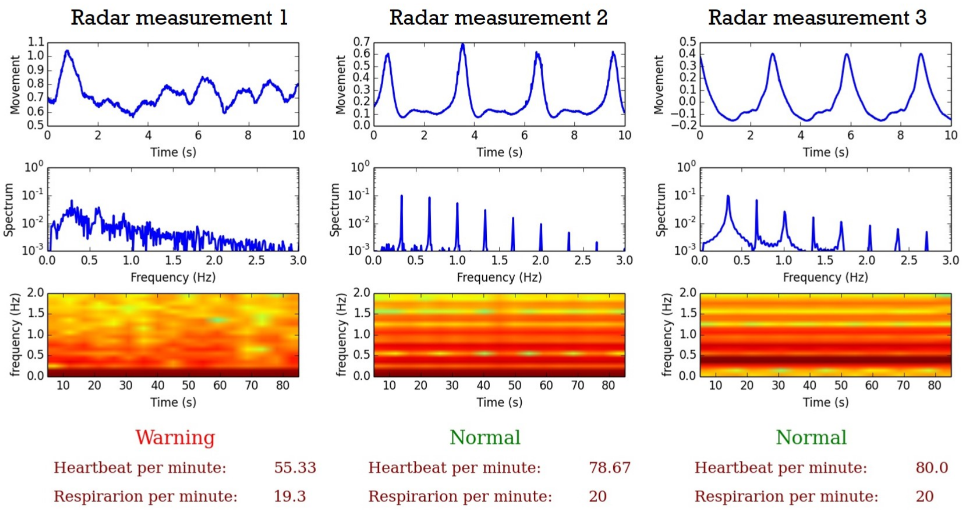

Figure 7.9. Testing if the systems detects dangerous situation and sets out a warning.

After proof of functionality of the systems, they are used to monitor three different people in three different rooms, however still, one of them is connected to traditional measurement tools. Figure 7.10 shows the result. The reference measurement tool shows 17 respiration per minute and 61 heart rate, while the radar system calculates 18 and 54 for those vital signs respectively.

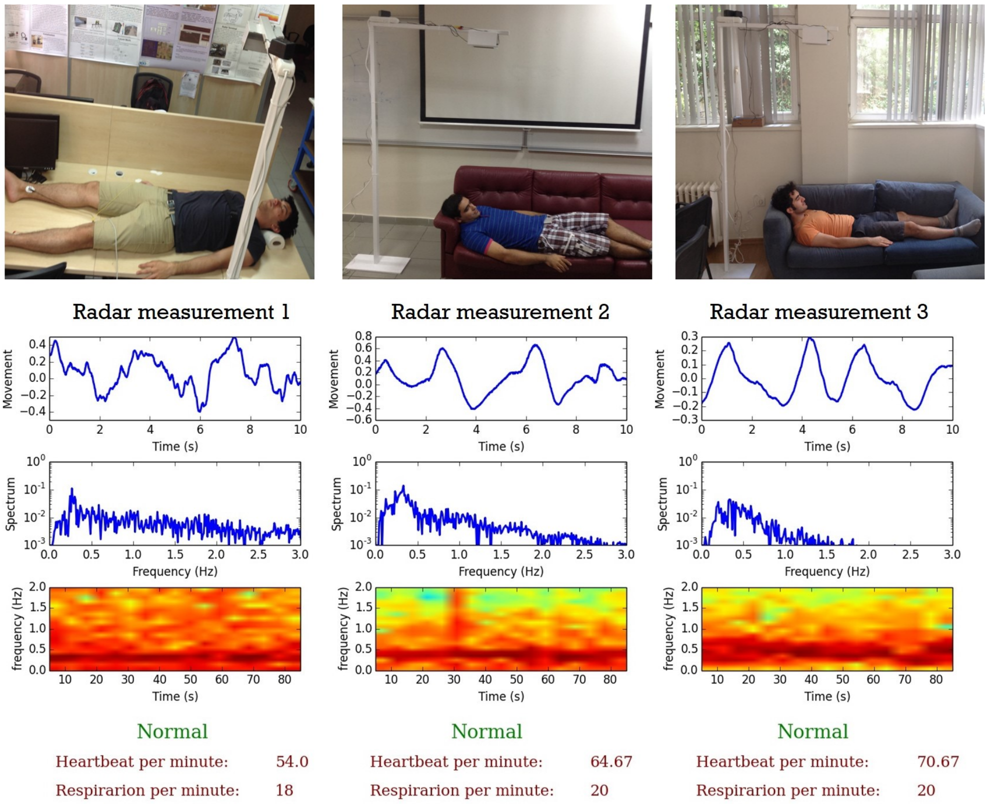

(a) Result of the proposed radar circuit.

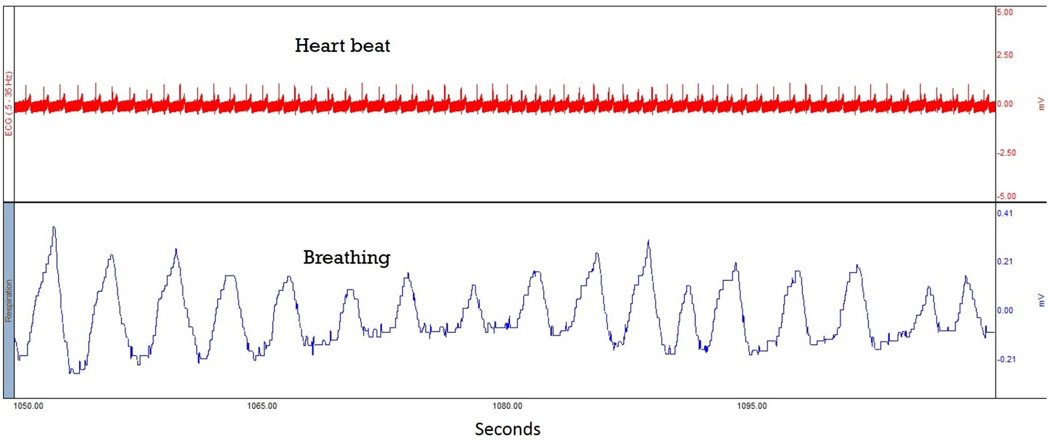

(b) Result of the reference device.

Figure 7.10. Measurement result for 3 patient simultaneously, the first one is checked with BIOPAC systems.

To further test the capabilities of the circuit, a 1.8 cm thick wooden surface is placed between radar circuit and the patient. This time, the adjustment time is a little increased but eventually the vital signs are obtained. Reference measurement shows 20.5 respiration per minute and 74 heartbeats per minute, these numbers are generated 20.67 and 78.67 respectively by the radar system.

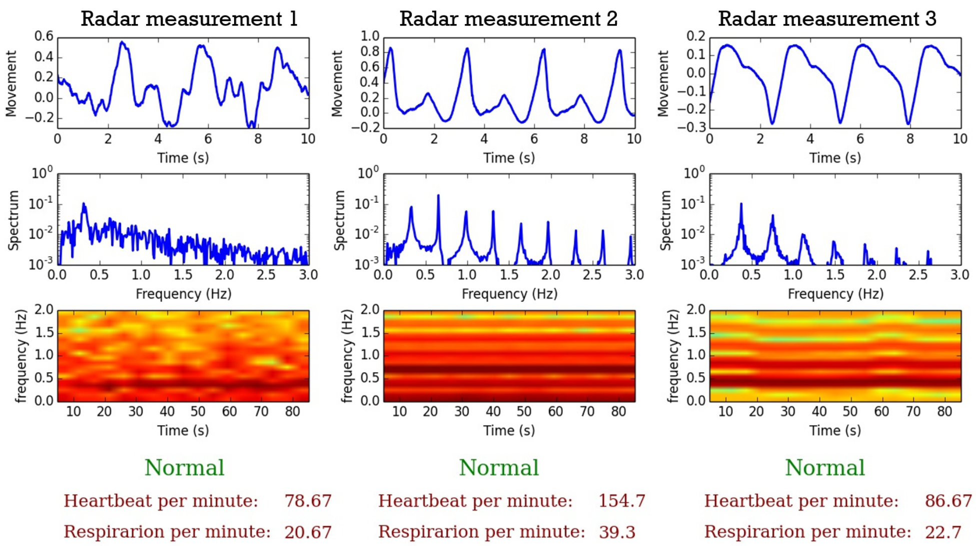

(a) Result of the proposed radar circuit.

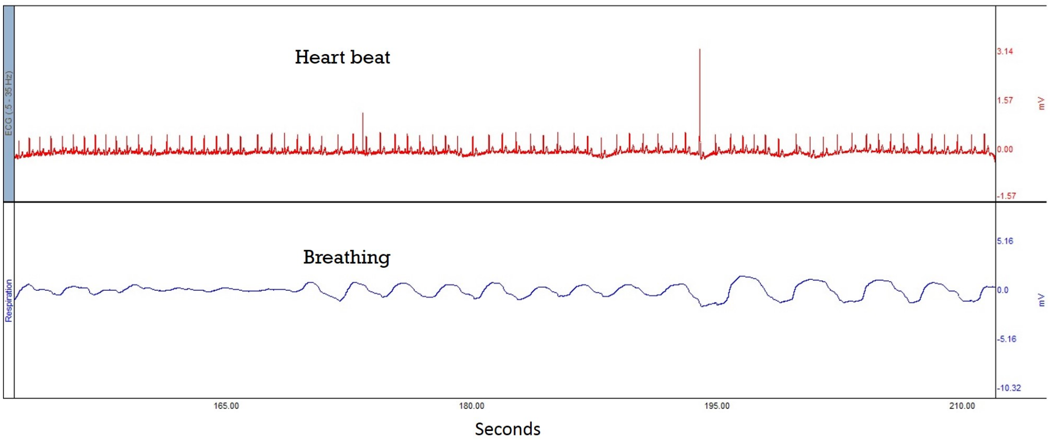

(b) Result of the reference device.

Figure 7.11. Measurement result for first patient sleeping under a wooden surface by thickness of 1.8 cm.

The measurement result is summarized in Table 7.1

Table 7.1. Measurement results.

Condition		Radar system measurement		Reference measurement		Error rate	
Distance (m)	Patient rotation	Respiratory rate (RPM)	Heart rate (BPM)	Respiratory rate(RPM)	Heart rate (BPM)	Breathing rate	Heart rate
1	Front	22	80	21.1	89	4.3%	10%
1	Back	19.7	74.67	21	60-92	6.2%	1.6%
1	Side	19.3	69.33	20	60-85	3.5%	4.37%
2	Front	22	64.67	20.5	40-68	7.3%	19.8%
1*	Front	20.67	78.67	20.5	74	0.8%	6.3%

*: The patient is sleeping under a 1.8 cm thick wooden object

8. CONCLUSIONS

To overcome uncomfortable or sometimes harmful traditional cardiorespiratory measurement tools for some patients, a K-band radar system for remote cardiorespiratory detection is successfully implemented. An accurate, fast response system to detect the respiration rate and the heart rate has been demonstrated. An analog circuitry is designed and fabricated to maintain SNR and amplitude, then after digitizing the data, digital signal processing steps are done to calculate wanted vital signs of the patient.

Stemmed results show correct functionality of the designed system, however, error rate is of characteristics of almost all electrical measurement devices. This device shows below 6.5 % error for respiration rate when the distance between patient and the radar system is below 1 m. The error increases to 7.5 % when distance is increased to two meters. Heart rate is changing with time. In the experiments, the instantaneous heart rate of the patient is recorded to be changing up to 40 % according to reference measurements. However, the obtained result from the radar system is less than 10 % faulty for distances below 1 m. Heart rate error increases as distance increases. The error for 2 m distance is recorded as 20 %.

When patient is placed under a thin barrier (which may actually happen in real life, consider early born infants), the radar system detects weak signals from chest of the patient, that is why it takes longer for system to adapt itself to the condition. However, the vital signs still can be. The error rate for similar condition is measured to be 0.5 % for respiration rate and 6.3 % for heart rate.

In case of this system, there are ways to reduce error and increase speed of the system. This system can be used for both sleeping and sitting patients, but sleeping patients provide more accurate life signs. Lying on back increases the robustness of the result and caretaker needs to make sure the package holder does not shake due to different reasons. The system must exactly look at the patient's chest and having conversation with patient, eating, or any extra movements decreases the precision of the obtained results.

During testing the circuit for functionality approval, it could be seen that even ECG and respiratory measurement belt, need to be tested on motionless patient to work as desired and generate trustworthy results. Movements affect the result, no matter what measurement mean is used.

While testing two methods together, the respiratory measurement belt, absorbs some chest wall movements (mostly vibrations in higher frequencies such as heartbeat) and inevitably weakens the heartbeat signal that we want to monitor. The heartbeat for patients without respiratory measurement belt is slightly more visible.

In this research, a K-band sensor interface design for remote cardiorespiratory sensing and monitoring has been successfully realized. The required research for monitoring the health condition has not been done in this work. Future work could include testing the system inside a hospital and do the patient monitoring. Using data from different patients, big steps could be taken toward illness diagnosis.

Steps remaining to reach mass production of this biomedical device are very short. Using more complicated network architectures to enable the server to receive from numerous terminals and improving signal processing to reduce the existing errors would almost make the system ready for mass production and their usage in everyday lives, thus taking a step to make health-care easier and more comfortable for everybody.

REFERENCES

1. Roopa.G, K.Rajanna and M. Nayak, “Non-invasive Human Breath Sensor”, *IEEE Sensors*, pp. 1788 – 1791, 2011.

2. Tan, K. S., R. Saatchi, H. Elphick and D. Burke, “Real-time Vision Based Respiration Monitoring System”, *2010 7th International Symposium on Communication Systems Networks and Digital Signal Processing (CSNDSP)*, pp. 770 – 774, 2010.

3. Gabriel, S., R. W. Lau and C. Gabriel, “The Dielectric Properties of Biological Tissues: III. Parametric Models for the Dielectric Spectrum of Tissues”, *Physics in Medicine and Biology*, Vol. 41, No. 11, p. 2271, 1996.

4. Aardal, O., Y. Paichard, S. Brovoll and T. Berger, “Physical Working Principles of Medical Radar”, *IEEE Transactions on Biomedical Engineering*, Vol. 60, No. 4, pp. 1142 – 1149, 2013.

5. Skolnik, M., *Introduction to Radar Systems*, McGraw-Hill, Inc., New York, NY, USA, 2002.

6. Pozar, D. M., *Microwave Engineering*, Wiley, Inc., Bognor Regis, West Sussex, UK, 2011.

7. Immoreev, I. I., N. J. Mohamed, J. D. Taylor, R. Vasquez, B. C. Flores, T. E. McEwan, J. B. Mendola, R. B. James, P. D. Hoffmeyer, R. M. Narayanan *et al.*, “Ultra-Wideband Radar Technology”, *CRC PRESS, London*, pp. 16–19, 2001.

8. Fukuchi, T. and T. Shiina, *Industrial Applications of Laser Remote Sensing*, Bentham Science, Inc., 2012.

9. Ye, H., “Life Detection Technique in Earthquake Search and Rescue”, *2012 Second International Conference on Instrumentation and Measurement, Computer,*

Communication and Control, pp. 664 – 666, 2012.

10. Xiao, Y., J. Lin, O. Boric-Lubecke and V. M. Lubecke, "A Ka-Band Low Power Doppler Radar System for Remote Detection of Cardiopulmonary Motion", *Engineering in Medicine and Biology 27th Annual Conference*, pp. 7151 – 7154, 2005.

11. Droitcour, A., V. Lubecke, J. Lin and O. Boric-Lubecke, "A Microwave Radio for Doppler Radar Sensing of Vital Signs", *Engineering in Medicine and Biology 27th Annual Conference*, Vol. 1, pp. 175 – 178, 2001.

12. Postolache, O., P. S. Girão, E. Lunca and P. Bicleanu, "Unobtrusive Cardio-Respiratory Monitoring Based on Microwave Doppler Radar", *International Conference and Exposition on Electrical and Power Engineering*, pp. 597 – 600, 2012.

13. Izadi, A., Z. Ghatan, B. Vahdat and F. Farzaneh, "Design and Simulation of a Life Detection System Based on Detection of the Heart Beat Using Doppler Frequency", *2006 IEEE International Symposium on Signal Processing and Information Technology*, pp. 685 – 690, 2006.

14. Kiaghadi, A., D. Teker, B. Enginoglu and A. Oncu, "A K-Band Radar System for Remote Cardiorespiratory Monitoring", *15th International Radar Symposium (IRS)*, 2014.

15. Rao, K. M. and B. Sudarshan, "A Review on Different Technical Specifications of Respiratory Rate Monitors", *International Journal of Research in Engineering and Technology*, Vol. 04, No. 04, pp. 424 – 429, 2015.

16. Association of Surgical Technologists, *Surgical Technology for the Surgical Technologist: A Positive Care Approach*, Delmar Cengage Learning, 2012.

17. Weigt, S. S., M. Abrazado, E. Kleerup, D. P. Tashkin and C. B. Cooper, "Time Course and Degree of Hyperinflation with Metronome-paced Tachypnea in COPD Patients", *COPD Journal of Chronic Obstructive Pulmonary Disease*, Vol. 5,

No. 5, pp. 298–304, 2008.

18. Maxim Integrated, *ICL7662/Si7661 CMOS Voltage Converters*, 2008.

19. THAT Corporation, *Blackmer® Trimmable IC, Voltage Controlled Amplifiers*, 2008.